AUTHOR INFORMATION

Corresponding Authors

*E-mail: demizu@nihs.go.jp. Tel: + 81-3-3700-1141; Fax: + 81-3-3707-6950.

*E-mail: masaaki@nihs.go.jp. Tel: + 81-3-3700-1141; Fax: + 81-3-3707-6950.

Notes

The authors declare no competing financial interest.

ACKNOWLEDGMENTS

This study was supported, in part, by JSPS KAKENHI Grant Numbers 26460169 (Y.D.), 26670041 (Y.K.), and 25893038 (T.M.) and by a Grant-in-Aid from the Tokyo Biochemical Research Foundation (Y.D.).

ABBREVIATIONS

Akt, protein kinase B; CD, circular dichroism; CLSM, confocal laser scanning microscopy; ER, estrogen receptor; E2, 17β-estradiol; PERM, peptidomimetic estrogen receptor modulators; RCAS, receptor cofactor assay systems; R7, heptaarginine; TFE, 2,2,2-trifluoroethanol

REFERENCES

(1) Holst, F., Stahl, P. R., Ruiz, C., Hellwinkel, O., Jehan, Z., Wendland, M., Lebeau, A., Terracciano, L., Al-Kuraya, K., Jänicke, F., Sauter, G., and Simon, R. (2007) Estrogen receptor alpha (ESR1) gene amplification is frequent in breast cancer. *Nat. Genet. 39*, 655–660.

(2) Doisneau-Sixou, S. F., Cergio, C. M., Carroll, J. S., Hui, R., Musgrove, E. A., and Sutherland, R. L. (2003) Estrogen and antiestrogen regulation of cell cycle progression in breast cancer cells. *Endocrine-Related Cancer 10*, 179–186.

(3) Foster, J. S., Henley, D. C., Bukovsky, A., Seth, P., and Wimalasena, J. (2001) Multifaceted regulation of cell cycle progression by estrogen: regulation of Cdk inhibitors and Cdc25A independent of cyclin D1-Cdk4 function. *Mol. Cell. Biol. 21*, 794–810.

(4) Howell, S. J., Johnston, S. R., and Howell, A. (2004) The use of selective estrogen receptor modulators and selective estrogen receptor down-regulators in breast cancer. *Best Pract. Res. Clin. Endocrinol. Metab. 18*, 47–66.

(5) Deroo, B. J., and Korach, K. S. (2006) Estrogen receptors and human disease. *J. Clin. Invest. 116*, 561–570.

(6) Baumann, C. K., and Castiglione-Gertsch, M. (2007) Estrogen receptor modulators and down regulators. *Drugs 67*, 2335–2353.

(7) Demizu, Y., Okuhira, H., Motoi, H., Ohno, A., Shoda, T., Fukuhara, K., Okuda, H., Naito, M., and Kurihara, M. (2012) Design and synthesis of estrogen receptor degradation inducer based on a protein knockdown strategy. *Bioorg. Med. Chem. Lett. 22*, 1793–1796.

(8) Shoda, T., Okuhira, K., Kato, M., Demizu, Y., Inoue, H., Naito, M., and Kurihara, M. (2014) Design and synthesis of tamoxifen derivatives as a selective estrogen receptor down-regulator. *Bioorg. Med. Chem. Lett. 24*, 87–89.

(9) Early Breast Cancer Trialists' Collaborative Group (1992) Systemic treatment of early breast cancer by hormonal, cytotoxic, or immune therapy: 133 randomised trials involving 31 000 recurrences and 24 000 deaths among 75 000 women. *Lancet 339*, 71–85.

(10) Fisher, B., Costantino, J. P., Wickerham, D. L., Redmond, C. K., Kavanah, M., Cronin, W. M., Vogel, V., Robidoux, A., Dimitrov, N., Atkins, J., Daly, M., Wieand, S., Tan-Chiu, E., Ford, L., and Wolmark, N. (1998) Tamoxifen for prevention of breast cancer: Report of the national surgical adjuvant breast and bowel project P-1 study. *J. Natl. Cancer Inst. (Bethesda) 90*, 1371–1388.

(11) Bernstein, L., Deapen, D., Cerhan, J. R., Schwartz, S. M., Liff, J., McGann-Maloney, E., Perlman, J. A., and Ford, L. (1999) Tamoxifen therapy for breast cancer and endometrial cancer risk. *J. Natl. Cancer Inst. 91*, 1654–1662.

(12) Shang, Y., and Brown, M. (2002) Molecular determinants for the tissue specificity of SERMs. *Science 295*, 2465–2468.

(13) Arpino, G., Wiechmann, L., Osborne, C. K., and Schiff, R. (2008) Crosstalk between the estrogen receptor and the HER tyrosine kinase receptor family: molecular mechanism and clinical implications for endocrine therapy resistance. *Endocr. Rev. 29*, 217–233.

(14) Lin, S.-L., Yan, L.-Y., Zhang, X.-T., Yuan, J., Li, M., Qiao, J., Wang, Z.-Y., Sheng, J., and Sun, Q.-Y. (2010) ER-alpha36, a variant of ER-alpha, promotes tamoxifen agonist action in endometrial cancer cells via the MAPK/ERK and PI3K/Akt pathways. *PLoS One 5*, e9013.

(15) Demizu, Y., Nagoya, S., Shirakawa, M., Kawamura, M., Yamagata, N., Sato, Y., Doi, M., and Kurihara, M. (2013) Development of stapled short helical peptides capable of inhibiting vitamin D receptor (VDR)-coactivator interactions. *Bioorg. Med. Chem. Lett. 23*, 4292–4296.

(16) Heery, D. M., Kalkhoven, E., Hoare, S., and Parker, M. G. (1997) A signature motif in transcriptional co-activators mediates binding to nuclear receptors. *Nature 387*, 733–736.

(17) Hall, J. M., and McDonnell, D. P. (2005) Coregulators in nuclear estrogen receptor action: from concept to therapeutic targeting. *Mol. Interventions 5*, 343–357.

(18) Hall, J. M., Chang, C., and McDonnell, D. P. (2000) Development of peptide antagonists that target estrogen receptorβ-coactivator interactions. *Mol. Endocrinol. 14*, 2010–2023.

(19) Leduc, A.-M., Trent, J. O., Wittliff, J. L., Bramlett, K. S., Briggs, S. L., Chirgadze, N. Y., Wang, Y., Burris, T. P., and Spatola, A. F. (2003) Helix-stabilized cyclic peptides as selective inhibitors of steroid receptor-coactivator interactions. *Proc. Natl. Acad. Sci. U.S.A. 100*, 11273–11278.

(20) Galande, A. K., Bramlett, K. S., Trent, J. O., Burris, T. P., Wittliff, J. L., and Spatola, A. F. (2005) Protein inhibitors of LXXLL-based protein-protein interactions. *ChemBioChem 6*, 1991–1998.

(21) Phan, T., Nguyen, H. D., Göksel, H., Möcklinghoff, S., and Brunsveld, L. (2010) Phage display selection of miniprotein binders of the Estrogen receptor. *Chem. Commun. 46*, 8207–8209.

(22) Phillips, C., Roberts, L. R., Schade, M., Bazin, R., Bent, A., Davies, N. L., Moore, R., Pannifer, A. D., Pickford, A. R., Prior, S. H., Read, C. M., Scott, A., Brown, D. G., Xu, B., and Irving, S. L. (2011) Design and structure of stapled peptides binding to estrogen receptors. *J. Am. Chem. Soc. 46*, 8207–8209.

(23) Carraz, M., Zwart, W., Phan, T., Michalides, R., and Brunsveld, L. (2009) Perturbation of estrogen receptor α localization with synthetic nona-arginine LXXLL-peptide coactivator binding inhibitors. *Chem. Biol. 16*, 702–711.

(24) Tints, K., Prink, M., Neuman, T., and Palm, K. (2014) LXXLL peptide converts transportan 10 to a potent inducer of apoptosis in breast cancer cells. *Int. J. Mol. Sci. 15*, 5680–5698.

(25) Nakase, I., Akita, H., Kogure, K., Gräslund, A., Langel, Ü., Harashima, H., and Futaki, S. (2012) Efficient intracellular delivery of nucleic acid pharmaceuticals using cell-penetrating peptides. *Acc. Chem. Res. 45*, 1132–1139.

(26) Yamashita, H., Demizu, Y., Shoda, T., Sato, Y., Oba, M., Tanaka, M., and Kurihara, M. (2014) Amphipathic short helix-stabilized peptides with cell-membrane penetrating ability. *Bioorg. Med. Chem. 22*, 2403–2408.

(27) A tyrosine residue was attached to the N-terminus of the heptaarginine fragment, as it enabled the concentrations of the peptides to be determined.

nature COMMUNICATIONS

ARTICLE

Received 28 Dec 2013 | Accepted 25 Jul 2014 | Published 25 Sep 2014

DOI: 10.1038/ncomms5806

Sphingosine-1-phosphate promotes expansion of cancer stem cells via S1PR3 by a ligand-independent Notch activation

Naoya Hirata[1], Shigeru Yamada[1], Takuji Shoda[2], Masaaki Kurihara[2], Yuko Sekino[1] & Yasunari Kanda[1]

Many tumours originate from cancer stem cells (CSCs), which is a small population of cells that display stem cell properties. However, the molecular mechanisms that regulate CSC frequency remain poorly understood. Here, using microarray screening in aldehyde dehydrogenase (ALDH)-positive CSC model, we identify a fundamental role for a lipid mediator sphingosine-1-phosphate (S1P) in CSC expansion. Stimulation with S1P enhances ALDH-positive CSCs via S1P receptor 3 (S1PR3) and subsequent Notch activation. CSCs overexpressing sphingosine kinase 1 (SphK1), an S1P-producing enzyme, show increased ability to develop tumours in nude mice, compared with parent cells or CSCs. Tumorigenicity of CSCs overexpressing SphK1 is inhibited by *S1PR3* knockdown or S1PR3 antagonist. Breast cancer patient-derived mammospheres contain SphK1$^+$/ALDH1$^+$ cells or S1PR3$^+$/ALDH1$^+$ cells. Our findings provide new insights into the lipid-mediated regulation of CSCs via Notch signalling, and rationale for targeting S1PR3 in cancer.

[1] Division of Pharmacology, National Institute of Health Sciences, Setagaya-ku, Tokyo 158-8501, Japan. [2] Division of Organic Chemistry, National Institute of Health Sciences, Setagaya-ku, Tokyo 158-8501, Japan. Correspondence and requests for materials should be addressed to Y.K. (email: kanda@nihs.go.jp).

Growing evidence suggests that many types of cancer, including breast, lung and prostate cancer, are initiated from a small population of cancer stem cells (CSCs; also called tumour-initiating cells)[1–8]. This minor population produces the bulk of cancers through continuous self-renewal and differentiation, which contributes to cancer heterogeneity. Therefore, it is essential to elucidate the signalling and regulatory mechanisms that are unique to CSCs, and to design novel therapeutic agents against CSCs.

CSCs have been isolated from diverse tumours and established cell lines, using several methods encompassing cell surface markers, aldehyde dehydrogenase (ALDH) activity, side population (SP) and sphere-forming ability. ALDH assays rely on the fact that the level of ALDH, a detoxifying enzyme responsible for the oxidation of intracellular aldehydes, is higher in stem cells than in differentiated cells[4]. ALDH1 expression is correlated with poor clinical prognosis in various cancers, such as breast, lung and prostate cancer[4–6]. Because CSCs have been considered to have molecular similarities to embryonic and normal adult stem cells, the self-renewal behaviour of CSCs has been reported to be mediated by several signalling pathways, such as Notch, Hedgehog and Wnt[9]. However, the molecular mechanisms that regulate the frequency and maintenance of CSCs via self-renewal signals remain poorly understood.

Autocrine and paracrine signalling plays a key role in maintaining the stem cell state and expansion of stem cells[10]. We therefore speculated that receptors for autocrine/paracrine factors might play a key role in CSC regulation. Using microarray screening in an ALDH-positive cell population of human breast cancer MCF-7 cells, we found that several receptors are upregulated. Among them, on the basis of pathophysiological properties, we focused on S1P receptor 3 (S1PR3), a receptor for a lipid mediator sphingosine-1-phospahate (S1P). S1P is known to exert multiple responses, such as proliferation, survival and cytoskeletal rearrangement, via its G protein-coupled receptor (GPCR) in many cell types[11]. S1P is synthesized from sphingosine by sphingosine kinase (SphK); two isoforms of mammalian SphK (sphingosine kinase 1 (SphK1) and SphK2) have been cloned and characterized[12,13]. In addition, the SphK1/S1P pathway has also been implicated in tumour progression[14,15]. S1P has also been shown to accumulate in the tumour microenvironment[16]. Although lipid mediators in cancer have been studied extensively, the role(s) of SphK1/S1P in CSCs remain unclear.

We demonstrate here that S1P regulates expansion of CSCs in several types of cancer. Our findings suggest that Notch activation is essential for S1P-induced proliferation of CSCs via S1PR3. We show that SphK1 regulates the tumorigenicity of breast CSCs via S1PR3. Using clinical samples, we show that breast cancer patient-derived CSCs contain SphK1$^+$/ALDH1$^+$ cells or S1PR3$^+$/ALDH1$^+$ cells. Thus, these results implicate the S1P signalling pathway as therapeutic targets in CSCs.

Results

S1P is a regulator of CSC population via S1PR3. We used an ALDH assay system to study the signalling pathways that regulate the frequency and maintenance of CSCs. Many cancer cell lines, including oestrogen receptor-positive MCF-7 cells, are known to contain an ALDH-positive cell population[5,6,17,18]. Consistent with a previous report[4], we confirmed that ALDH-positive cell population in MCF-7 cells possessed CSC-like properties, as assessed by expression of stem cell markers, drug resistance and tumorigenicity (Supplementary Fig. 1). Through microarray analysis, we investigated a possible receptor that increases the proportion of the ALDH-positive cell population in MCF-7 cells as a CSC model. We found *S1PR3* as a possible candidate in CSC regulation (Supplementary Data 1). *S1PR3* was highly expressed in the ALDH-positive cell population, a finding confirmed by quantitative polymerase chain reaction (qPCR) assays (Fig. 1a). *S1PR2* expression was lower in the ALDH-positive cell population compared with MCF-7 cells, and other types of *S1PR* are yet to be detected in MCF-7 cells (Supplementary Fig. 2)[19,20]. Stimulation with S1P increased the proportion of ALDH-positive cell population in a dose-dependent manner, with a maximal response observed at 100 nM (Fig. 1b). Similar to S1P, dihydro-S1P, another S1PR3 ligand, also increased the ALDH-positive cell population (Supplementary Fig. 3). Moreover, stimulation with S1P increased the number of SP cells (Fig. 1c), mammosphere-forming efficiency (Fig. 1d), CD44$^+$/CD24$^-$ population (Fig. 1e) and expression of stem cell markers (Fig. 1f). These data indicate that stimulation with S1P leads to an increase in breast CSCs. In contrast, lysophosphatidic acid (LPA), another well-studied lipid mediator, did not increase CSCs in MCF-7 cells. To confirm the involvement of S1PR3, we inhibited S1PR3 using pharmacological antagonists and RNA interference techniques. The effects of S1P were blocked by the S1PR3 antagonist TY52156 (ref. 21). Another antagonist CAY10444, which is structurally different from TY52156, also inhibited the S1P effect. In contrast, the S1PR2 antagonist JTE013 had little effect (Fig. 1g). Experiments using small interfering RNAs (siRNA) confirmed the effects of antagonists (Fig. 1h). In addition, short hairpin RNAs (shRNAs) against *S1PR3* also inhibited the enhancement of mammosphere-forming ability by S1P (Supplementary Fig.4). Similar results with ALDH assay were obtained in triple-negative MDA-MB-231 cells (Supplementary Fig. 5a,b), suggesting that S1P regulates both luminal and triple-negative type of breast CSCs. Furthermore, we examined CSCs from other tumour types to determine whether these effects of S1P are limited to breast cancer cell lines. Similar to MCF-7 cells, stimulation with S1P increased the ALDH-positive cell population in human lung cancer A549 cells, human prostate cancer LNCaP cells, human glioma U251MG cells and human ovarian cancer OVCAR-5 cells (Supplementary Fig. 6a). In addition, TY52156 inhibited the S1P effect in these cell lines. Taken together, these data demonstrate that S1P has an ability to increase the number of CSCs via S1PR3 in several types of cancer.

S1P enhances Notch signalling via S1PR3. Growing evidence suggests many similarities between embryonic stem cells and CSCs[9]; therefore, we focused on Notch, Hedgehog and Wnt as signalling pathway candidates downstream of the S1PR. Stimulation with S1P induced expression of the Notch target gene *Hes1* in MCF-7 cells (Fig. 2a) and ALDH-positive MCF-7 cells (Supplementary Fig. 7a). Moreover, S1P also induced the *Hes1* expression in ALDH-positive A549, LNCaP, U251 and OVCAR-5 cells (Supplementary Fig. 7b). S1P-induced *Hes1* expression was inhibited by S1PR3 antagonists (Fig. 2b). In contrast, the Hedgehog target gene *Gli1*, and Wnt target gene *Dkk1* were not induced. The effect of S1P on ALDH-positive cell population was inhibited by DAPT, an inhibitor of γ-secretase, which has multiple substrates including Notch, not by the Hedgehog inhibitor cyclopamine and the Wnt inhibitor PNU74654 (Fig. 2c; Supplementary Fig. 8). Similar effects of DAPT were obtained in MDA-MB-231 cells (Supplementary Fig. 5d), A549 cells, LNCaP cells, U251 cells and OVCAR-5 cells (Supplementary Fig. 6b). To determine whether S1P has the ability to activate the Notch pathway, we examined cleavage of Notch in MCF-7 cells. Stimulation with S1P produced the Notch intracellular domain (N1ICD) (Fig. 2d) and induced activation of the Notch transcriptional reporter *CSL*-luc (Fig. 2e). Because *Hes1* expression is dependent on NICD/CSL/MAML

complex-mediated gene transcription[22], we verified whether co-activators were involved in CSCs, using dominant-negative (DN) mutants of CSL, which have been reported to have no ability to bind to DNA[23]. DN-CSL inhibited S1P-induced *Hes1* expression and the ALDH-positive cell population (Fig. 2f). Similar results were obtained by DN-MAML, which lacks transcriptional activating domain and inhibits NICD-dependent transcriptional activition[24]. To examine which subtype of Notch was involved in CSCs, we overexpressed each type of NICD. Overexpression of N1ICD increased *Hes1* expression and the ALDH-positive cell population (Fig. 2g). N3ICD also increased the ALDH-positive cell population (Supplementary Fig. 9a), while N2ICD and

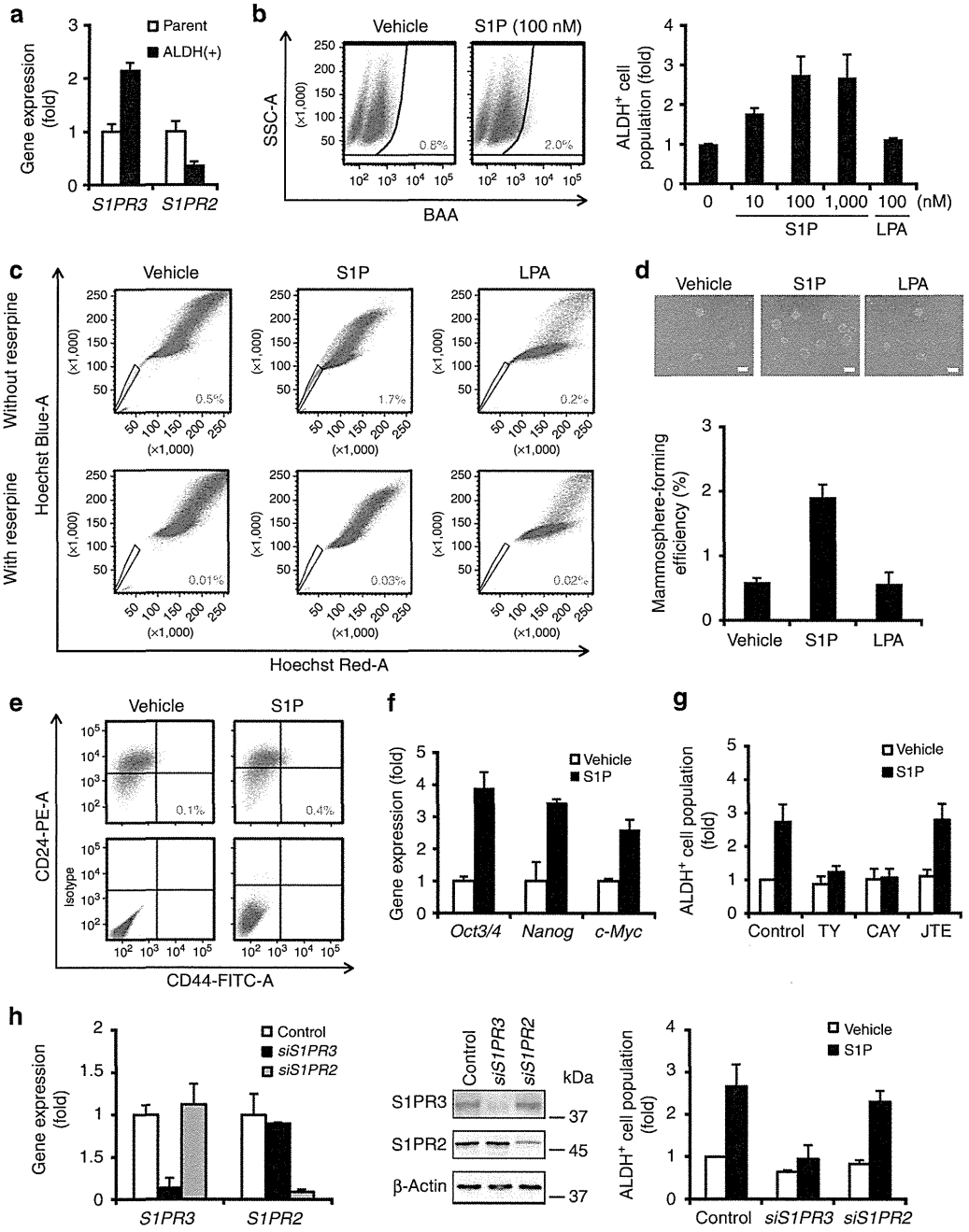

Figure 1 | Role of S1PR3 in the ALDH-positive cell population within the MCF-7 cell line. (**a**) Expression levels of S1PR (*S1PR2* and *S1PR3*) in parental or ALDH-positive MCF-7 cells by qPCR. Data represent mean ± s.d. ($n=3$). (**b**) Representative flow data with ALDH substrate in the presence or absence of S1P (100 nM, 3 days) in MCF-7 cells. Dose-dependent effects of S1P in the proportion of ALDH-positive cell population. Data represent mean ± s.d. ($n=3$). (**c**) Representative flow data of the SP assay with Hoechst 33342 dye alone or in the presence of reserpine (15 μg ml^{-1}). (**d**) Effects of S1P (100 nM) on mammosphere-forming efficiency in MCF-7 cells. The number of mammospheres was microscopically counted and the percentage of mammosphere-forming cells was determined as mammosphere-forming efficiency (%). The scale bar, 100 μm. Data represent mean ± s.d. ($n=3$). (**e**) Effects of S1P (100 nM) on CD44$^+$/CD24$^-$ population in MCF-7 cells. (**f**) Effects of S1P (100 nM) on expression of stem cell markers by qPCR. Data represent mean ± s.d. ($n=3$). (**g**) Effects of S1PR3 antagonists (TY52156, 1 μM; CAY10444, 10 μM) and the S1PR2 antagonist (JTE013, 10 μM) on S1P-induced increase in the ALDH-positive cell population. Data represent mean ± s.d. ($n=3$). (**h**) After transfection with siRNA, expression levels of S1P receptor were examined by qPCR and immunoblotting. Effects of siRNAs against *S1PR3* and *S1PR2* on S1P-induced increase in the ALDH-positive cell population. Data represent mean ± s.d. ($n=3$). Expression levels were normalized to glyceraldehyde 3-phosphate dehydrogenase messenger RNAs.

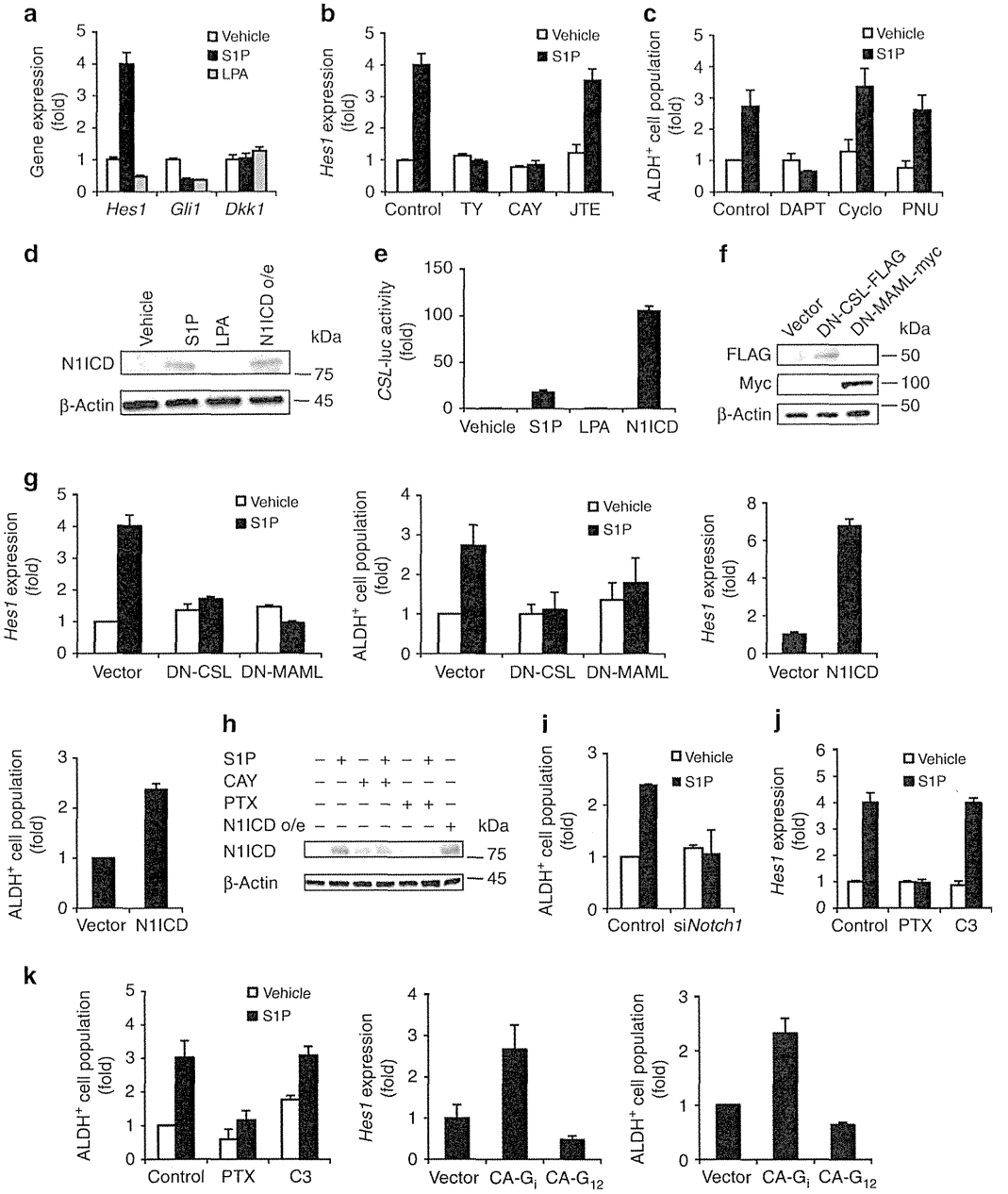

Figure 2 | Role of Notch signalling in ALDH-positive cell population. (**a**) After stimulation with S1P (100 nM) or LPA (100 nM) for 24 h, expression levels of the Notch target gene (*Hes1*), Hedgehog target gene (*Gli1*) and Wnt target gene (*Dkk1*) were quantified in MCF-7 cells using qPCR. Data represent mean ± s.d. ($n=3$). (**b**) Effects of TY52156 (1 μM) or CAY10444 (10 μM) on S1P-induced *Hes1* expression using qPCR. Data represent mean ± s.d. ($n=3$). (**c**) Effects of the Notch inhibitor DAPT (5 μM), the Hedgehog inhibitor cyclopamine (10 μM) or the Wnt inhibitor PNU74654 (10 μM) on S1P-induced increase in the ALDH-positive cell population. Data represent mean ± s.d. ($n=3$). (**d**) Effects of S1P or LPA on N1ICD production by immunoblotting. (**e**) MCF-7 cells transfected with a reporter plasmid encoding CSL-luc were cultured with or without S1P or LPA and were then analysed by luciferase assays. Data represent mean ± s.d. ($n=3$). (**f**) Effects of overexpression of Flag-tagged DN-CSL or myc-tagged DN-MAML on S1P-induced *Hes1* expression and ALDH-positive cell population. Data represent mean ± s.d. ($n=3$). The expression of plasmids was analysed by immunoblotting using tag-specific antibodies. (**g**) Effects of overexpression of N1ICD on *Hes1* expression and ALDH-positive cell population. Data represent mean ± s.d. ($n=3$). (**h**) After pretreatment with PTX (0.1 μg ml^{-1}, 24 h) or CAY10444 (10 μM, 30 min), the cells were stimulated with S1P. N1ICD production was analysed by immunoblotting with N1ICD-specific antibodies. (**i**) Effects of siRNA against *Notch1* on S1P-induced increase in the ALDH-positive cell population. Data represent mean ± s.d. ($n=3$). (**j**) Effects of toxins (PTX, 0.1 μg ml^{-1}; C3 Toxin, 0.1 μg ml^{-1}) on S1P-induced *Hes1* expression and ALDH-positive cell population. Data represent mean ± s.d. ($n=3$). (**k**) Effects of overexpression of CA mutants of G_i or G_{12} on S1P-induced *Hes1* expression and ALDH-positive cell population. Data represent mean ± s.d. ($n=3$). Expression levels were normalized to glyceraldehyde 3-phosphate dehydrogenase messenger RNAs.

N4ICD had little effect. S1P-induced N1ICD production was inhibited by CAY10444 (Fig. 2h); however, S1P did not induce N3ICD production (Supplementary Fig. 9b). To further examine the involvement of Notch in CSC, we performed knockdown experiments using *Notch1* siRNA. Knockdown of *Notch1* inhibited the effect of S1P on ALDH-positive cell population (Fig. 2i; Supplementary Fig. 10). Taken together, these data suggest crosstalk between S1P and Notch1. To confirm the

involvement of S1PR3 in crosstalk, we studied subtype of G proteins coupled to S1PR3. Pertussis toxin (PTX), which inactivates G_i protein, abolished S1P-induced *Hes1* expression and the ALDH-positive cell population, whereas C3 toxin, which inactivates an effector of $G_{12/13}$ Rho, had little effect (Fig. 2j). The effects of toxins were confirmed by overexpression of constitutively active (CA) mutants for G_i, but not by CA-G_{12} (Fig. 2k). These data suggest that G_i mediates S1P-induced Notch activation via S1PR3. Collectively, S1P has an ability to increase the number of CSCs via Notch signalling in several types of cancer.

S1P increases ADAM17 activity without Notch ligands. We further investigated the molecular mechanism of crosstalk between S1P and Notch in MCF-7 cells. Notch is generally activated by binding of Notch ligands to Notch and then cleaved by ADAM17 and γ-secretase[25]. Among Notch ligands (Jagged1, 2 and Delta-like ligand (Dll) 1, 3 and 4), Dll3 is not capable to activate Notch signalling in adjacent cells[26].

To examine whether Notch ligands are required for the S1P effect, we examined the expression level of Notch ligands. S1P did not induce expression levels of Notch ligands (Supplementary Fig. 11a). Knockdown of Notch ligands did not affect S1P-induced *Hes1* expression and ALDH-positive cell population (Fig. 3a,b). In contrast to S1P, knockdown of Notch ligands inhibited hypoxia-mimetic agent desferoxamine-induced *Hes1* expression. In addition, neutralizing antibodies to Jagged1 inhibited *Hes1* induction by soluble Jagged1-Fc, but not S1P-induced *Hes1* expression and ALDH-positive cell population (Supplementary Fig. 11c,d). Taken together, these data suggest that S1P activates Notch signalling in Notch ligand-independent manner.

We next studied cleavage enzymes that are responsible for S1P-induced Notch activation. We found that stimulation with S1P increased ADAM17 activity in MCF-7 cells (Fig. 3c) and ALDH-positive MCF-7 cells (Supplementary Fig. 7c). In addition, S1P also increased γ-secretase activity in MCF-7 cells (Supplementary Fig. 12a). CAY10444 and PTX inhibited S1P-induced ADAM17 activation (Fig. 3d) and γ-secretase activation (Supplementary Fig. 12b). Overexpression of CA-G_i also increased both ADAM17 (Fig. 3e) and γ-secretase activity (Supplementary Fig. 12c). Moreover, we examined whether ADAM17 activation occurred in CSCs. Overexpression of ADAM17 increased N1ICD production, *Hes1* expression and the ALDH-positive cell population (Fig. 3f). Conversely, DN-ADAM17 (E406A; point mutation at metalloprotease domain)[27] inhibited S1P-induced responses (Fig. 3g). Expression of ADAM10 or DN-ADAM10 (E384A; point mutation at metalloprotease domain)[28] had little effect on the CSC signalling pathway. These data suggest that ADAM17 is involved in S1P-induced CSC proliferation.

p38MAPK mediates ADAM17 activation by S1P. We investigated whether the intracellular domain of ADAM17 plays a role in S1P-induced breast CSC proliferation. ADAM17 activity is regulated by phosphorylation-dependent mechanisms[29–31]; therefore, we generated ADAM17 mutants with either Thr735 (p38MAPK consensus motif) or Thr761 (Akt consensus motif) replaced by alanine (Fig. 4a). Consistent with our data above, S1P induced ADAM17 phosphorylation at Thr735 (Fig. 4b). S1P-induced ADAM17 phosphorylation was inhibited by PTX and CAY10444. A mutation at Thr735 decreased ADAM17 phosphorylation through S1P, whereas a mutation at Thr761 had little effect (Fig. 4c). In addition, mutation of Thr735 inhibited S1P-induced ADAM17 activation, *Hes1* expression and the number of ALDH-positive cell population (Fig. 4d). To further confirm the involvement of p38MAPK, we studied the association between p38MAPK and ADAM17. Stimulation with S1P induced a transient phosphorylation of p38MAPK (Supplementary Fig. 13a) and an association between p38MAPK and ADAM17 (Fig. 4e). Mutation of Thr735 abolished this association (Fig. 4f), suggesting that phospho-p38MAPK binds to ADAM17 at Thr735. Treatment with CAY10444 or PTX also inhibited the S1P-induced association between p38MAPK and ADAM17 (Fig. 4g). The p38MAPK inhibitor SB203580 inhibited the S1P-induced responses (Supplementary Fig. 13b–d). Furthermore, SB203580 inhibited the association between p38MAPK and ADAM17 (Supplementary Fig. 13f). In contrast, the PI3-kinase/Akt pathway inhibitor LY294002 had little effect (Supplementary Fig. 13b–e). Taken together, these data suggest that p38MAPK-mediated ADAM17 activation is involved in the S1P-induced CSC phenotype.

SphK1 increases CSCs via S1PR3. S1P is synthesized through SphK-catalyzed phosphorylation of sphingosine[11,14]. We next examined whether SphK is involved in breast CSCs. Consistent with previous reports[32,33], overexpressed SphK1 was localized in the cytosol, and SphK2 was mainly localized to the nucleus (Fig. 5a). Enzyme activities of SphKs were also confirmed (Supplementary Fig. 14). Overexpression of SphK1 increased the number of ALDH-positive cell population in both MCF-7 (Fig. 5b) and MDA-MB-231 cells (Supplementary Fig. 15), whereas SphK2 had little effect. Consistent with the ALDH assay results, ADAM17 activation, N1ICD production and *Hes1* expression were induced by SphK1 but not SphK2 (Fig. 5c). To determine whether intracellular S1P is involved in the SphK1 effect, we tested the effects of the S1PR3 antagonist on SphK1-induced increases in the ALDH-positive cell population. Pretreatment with CAY10444 inhibited SphK1-induced responses (Fig. 5d). *S1PR3* shRNAs also inhibited these SphK1-induced responses (Fig. 5e). Analysis by qPCR confirmed specific suppression of *S1PR3* by these shRNAs (Fig. 5e), and treatment with PTX also produced similar results. Recent studies suggest that the ABC transporter mediates oestrogen-induced S1P secretion in MCF-7 cells[34]. To determine whether the ABC transporter is involved with the SphK1 effect, we used siRNAs and a selective inhibitor to inhibit the transporter. An siRNA against *ABCC1* inhibited SphK1-induced ADAM17 activation, *Hes1* expression and the ALDH-positive cell population (Supplementary Fig. 16a). The ABCC1 inhibitor MK571 also produced similar results (Supplementary Fig. 16b). In contrast, an siRNA against *Spns2*, another S1P transporter[35], had little effects. These data suggest that S1P produced by SphK1 stimulates S1PR3, and leads to an increase in the number of CSCs.

SphK1 accelerates tumour formation of CSCs via S1PR3. Since S1P is easily degraded by S1P lyase or phosphatases, we next studied tumorigenicity using SphK1- or SphK2-overexpressing CSCs in MCF-7 cells. Almost all nude mice injected with SphK1-overexpressing ALDH-positive cells developed tumours within 6 weeks. Tumour formation was inefficient in the mice injected with vector- or SphK2-overexpressing ALDH-positive cells (Fig. 6a,b). Tumour sizes from SphK1-overexpressing ALDH-positive cells were bigger than those from vector- or SphK2-overexpressing ALDH-positive cells (Fig. 6c,d). Histological analysis indicated that tumours derived from the ALDH-positive cells and the SphK1-overexpressing ALDH-positive cells had similar morphologies (Fig. 6e). To examine the proportion of ALDH-positive cells in xenografted tumour samples, we conducted double staining using ALDH assays and human-specific antibodies to TRA-1-85 (Supplementary Fig. 17). The increase in

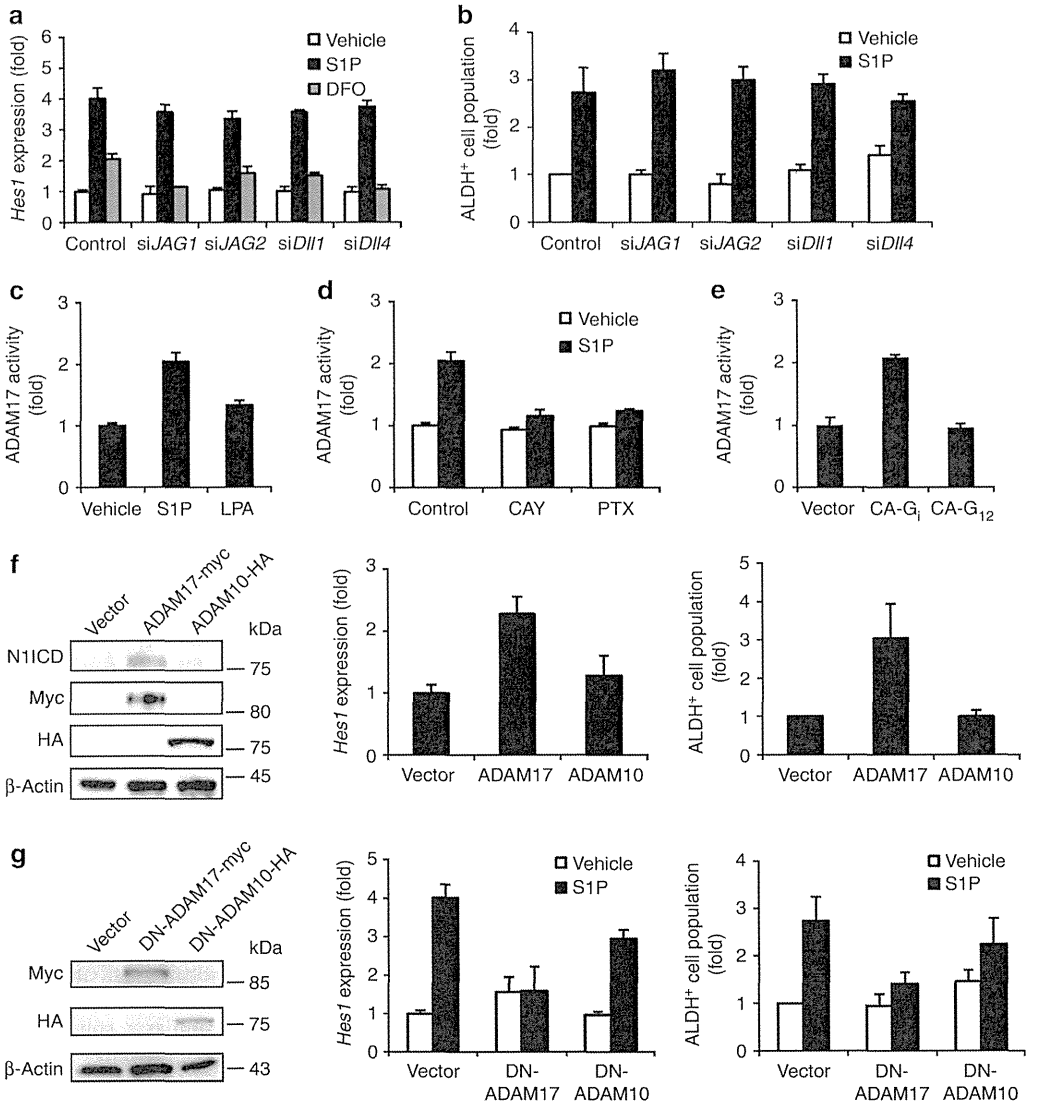

Figure 3 | S1P increases ALDH-positive cell population without Notch ligands. (**a**) Effects of siRNA against *Jagged1*, *Jagged2*, *Dll1* and *Dll4* on desferoxamine- or S1P-induced *Hes1* expression. Data represent mean ± s.d. ($n=3$). (**b**) Effects of siRNA against *Jagged1*, *Jagged2*, *Dll1* and *Dll4* on S1P-induced increase in ALDH-positive cell population. Data represent mean ± s.d. ($n=3$). (**c**) Stimulation with S1P (100 nM, 4 h) increased ADAM17 enzyme activity. Data represent mean ± s.d. ($n=3$). (**d**) S1P-induced ADAM17 activation was inhibited by CAY10444 (10 μM) and PTX (0.1 μg ml^{-1}). Data represent mean ± s.d. ($n=3$). (**e**) ADAM17 activation was induced by the overexpression of CA-G_i, but not by CA-G_{12}. Data represent mean ± s.d. ($n=3$). (**f**) Immunoblotting of N1ICD in ADAM17-myc- and ADAM10-HA-overexpressed MCF-7 cells. The expression of plasmids was confirmed using tag-specific antibody. Effects of overexpression of ADAM17 or ADAM10 on *Hes1* expression in MCF-7 cells. Effects of overexpression of ADAM17 or ADAM10 on ALDH-positive cell population in MCF-7 cells. Data represent mean ± s.d. ($n=3$). (**g**) Effects of DN mutants of ADAM17 or DN-ADAM10 on S1P-induced *Hes1* expression and the ALDH-positive cell population. Data represent mean ± s.d. ($n=3$). Expression levels were normalized to glyceraldehyde 3-phosphate dehydrogenase messenger RNAs.

the proportion of ALDH-positive cells in the tumour paralleled the *in vitro* results, suggesting a stem cell hierarchy (Fig. 6f). Histological analysis and double staining suggest that it is unlikely that the enhanced incidence of tumour formation by expression of SphK1 was due to cell differentiation. To examine whether S1PR3 and ALDH1 were co-expressed in the same cell, we performed double staining of ALDH1 and S1PR3 using xenografted tumour section (Supplementary Fig. 18). The number of ALDH1- and S1PR3 double-positive cells was increased in tumours derived from the SphK1-overexpressing ALDH-positive cells, compared with control and SphK2-overexpressing ALDH-positive cells. In addition, knockdown of *S1PR3* significantly inhibited the tumorigenicity of SphK1-overexpressing ALDH-positive cells, whereas knockdown of *S1PR2* had little effect (Fig. 6g). Furthermore, chronic administration of the S1PR3 antagonist TY52156 significantly inhibited the tumorigenicity of SphK1-overexpressing ALDH-positive cells (Fig. 6h). Taken together, both *in vitro* and *in vivo* results suggest that enhanced expression of SphK1 accelerated tumour formation of CSCs via S1PR3.

Patient-derived CSCs contain SphK1$^+$/ALDH1$^+$ cells. We further extended our observations to primary cell culture. To examine *S1PR3* expression level in breast CSCs, we performed qPCR using secondary mammospheres from patient-derived tumour[8] (Supplementary Table 1). Similar to MCF-7 cells, *S1PR3* was highly expressed in ALDH-positive cells derived from breast cancer patient (Fig. 7a). In addition, we evaluated whether there

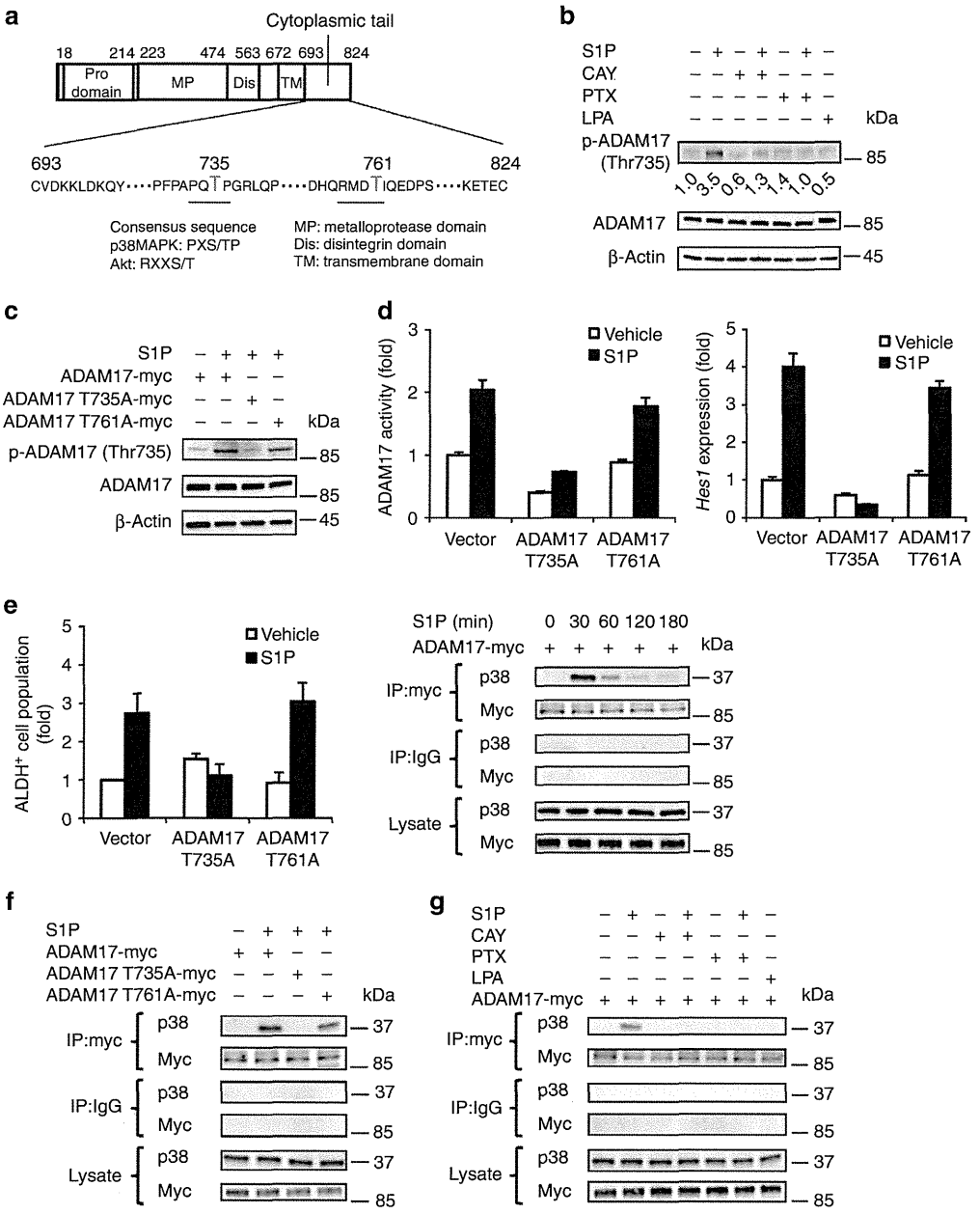

Figure 4 | S1P-induced ADAM17 activation via p38MAPK. (**a**) A schematic of the ADAM17 cytoplasmic domain mutants. (**b**) S1P-induced phosphorylation of ADAM17 at Thr735 was analysed by immunoblotting with a phospho-ADAM17 (Thr735)-specific antibody. (**c**) MCF-7 cells were transfected with ADAM17-T735A-myc or ADAM17-T761A-myc mutants and were then immunoblotted with phospho-ADAM17 (Thr735)-specific antibodies. (**d**) Effects of ADAM17-T735A and ADAM17-T761A mutants on S1P-induced ADAM17 activation, *Hes1* expression and ALDH-positive cell population. Expression levels were normalized to glyceraldehyde 3-phosphate dehydrogenase messenger RNAs. Data represent mean ± s.d. ($n=3$). (**e**) MCF-7 cells transfected with myc-tagged ADAM17 were either treated or untreated with S1P (100 nM) for the indicated times. The cells were then lysed and subjected immunoprecipitation with myc-specific antibodies, followed by p38MAPK-specific immunoblotting. (**f**) MCF-7 cells were transfected with myc-tagged ADAM17-T735A or T761A and stimulated with S1P (100 nM) for 30 min. The cells were then lysed and subjected to immunoprecipitation with myc-specific antibodies, followed by p38MAPK-specific immunoblotting. (**g**) MCF-7 cells transfected with myc-tagged ADAM17 were treated with S1P (100 nM) or LPA (100 nM) for 30 min in the presence or absence of CAY10444 (10 μM) or PTX (0.1 μg ml^{-1}). The cells were lysed and subjected to immunoprecipitation with myc-specific antibodies, followed by p38MAPK-specific immunoblotting.

were co-expressions of SphK1/ALDH1 or S1PR3/ALDH1 in breast CSCs by immunochemistry. Double staining demonstrated that these patient samples contained SphK1- and ALDH1 double-positive cells or S1PR3- and ALDH1 double-positive cells (Fig. 7b,c). We further evaluated whether SphK1, ADAM17 and N1ICD were co-expressed in the same cell. As a result, patient-derived tumour cells contained triple-positive cells (Fig. 7d). These data suggest that SphK1/S1PR3/Notch signalling is present in CSCs derived from breast cancer patient.

Discussion

In the present study, we used ALDH assays to identify regulators in CSCs, and determined that S1P/S1PR3 signalling and

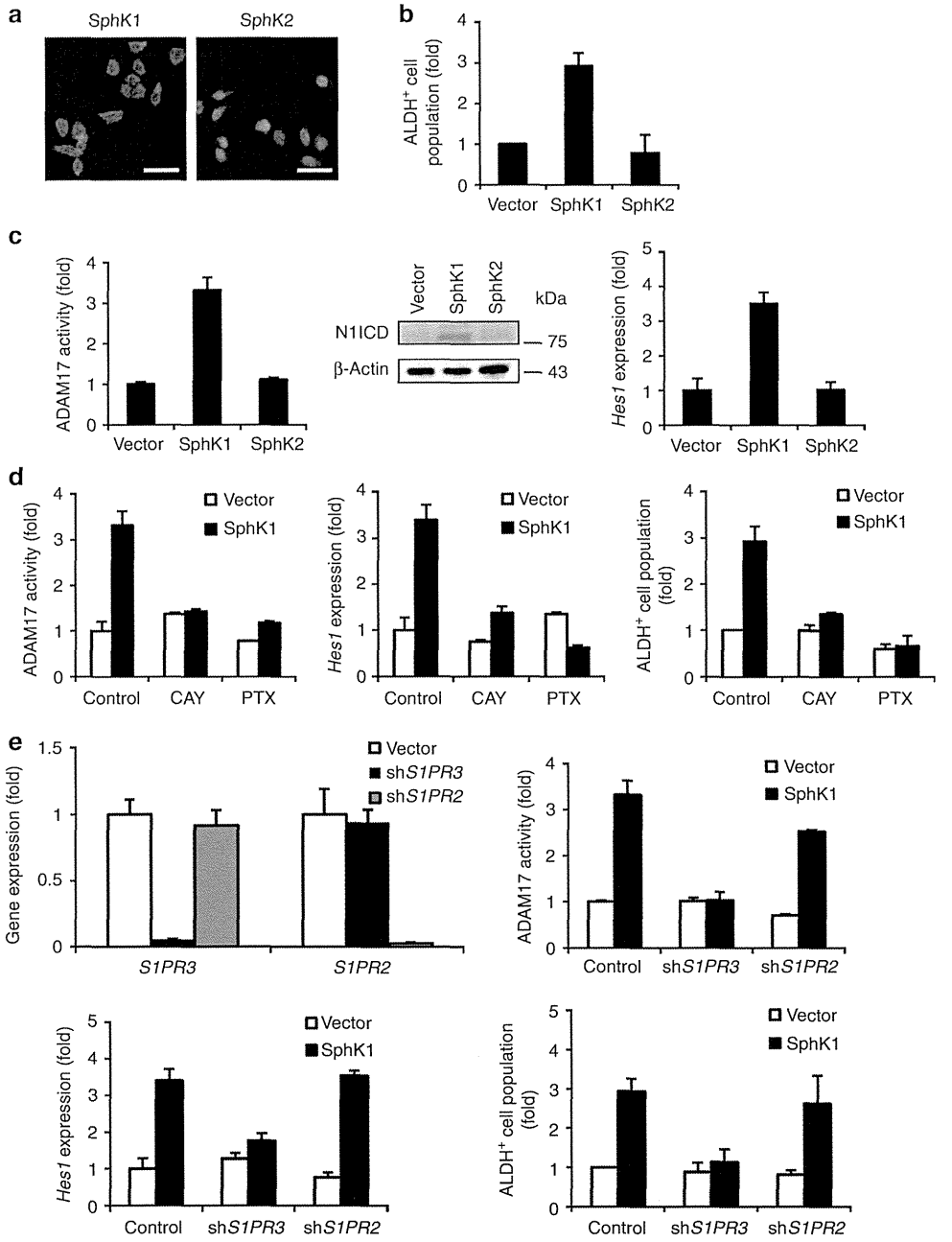

Figure 5 | Role of SphK1 in ALDH-positive cell population. (**a**) Expression of SphK in MCF-7 cells. Plasmid vectors encoding FLAG-tagged SphK1, or HA-tagged SphK2 were transfected into MCF-7 cells before SphK protein levels in cells were analysed by immunostaining. The scale bar indicates 20 μm. (**b**) Effects of SphK1 and SphK2 on the ALDH-positive cell population. Data represent mean ± s.d. ($n=3$). (**c**) Effects of SphK1 and SphK2 on ADAM17 activity, NICD production, and *Hes1* expression. Data represent mean ± s.d. ($n=3$). (**d**) Effects of CAY10444 (10 μM) and PTX (0.1 μg ml^{-1}) on the SphK1-induced ADAM17 activity, *Hes1* expression and ALDH-positive cell population. Data represent mean ± s.d. ($n=3$). (**e**) Expression level of S1P receptor in shRNA-transduced MCF-7 cells. Effects of shRNAs against *S1PR3* and *S1PR2* on the SphK1-induced ADAM17 activity, *Hes1* expression and ALDH-positive cell population. Data represent mean ± s.d. ($n=3$). Expression levels were normalized to glyceraldehyde 3-phosphate dehydrogenase messenger RNAs.

subsequent Notch activation resulted in an increase in the CSCs in several types of cancer (Fig. 8). S1PR3 antagonist inhibited the tumorigenicity of SphK1-overexpressed breast CSCs. Furthermore, breast cancer patient-derived CSCs contained SphK1$^+$/ALDH1$^+$ cells or S1PR3$^+$/ALDH1$^+$ cells. The findings presented here broaden our understanding of the role of lipids in CSC biology, and have significant clinical implications.

We found that S1P has the ability to induce proliferation of several types of CSCs, as stimulation with S1P activates Notch signalling, a key stem cell pathway. As such, S1P might have various roles in stem/progenitor cells. Indeed, S1P has been shown to maintain self-renewal of human embryonic stem cells in cooperation with platelet-derived growth factor[36]. Human-induced pluripotent stem cells have also been shown to express *S1PR3* messenger RNAs, although their biological effects in induced pluripotent stem cells are yet to be elucidated[37]. We postulate that S1P might have self-renewal properties, and play a key role in stem cell regulation.

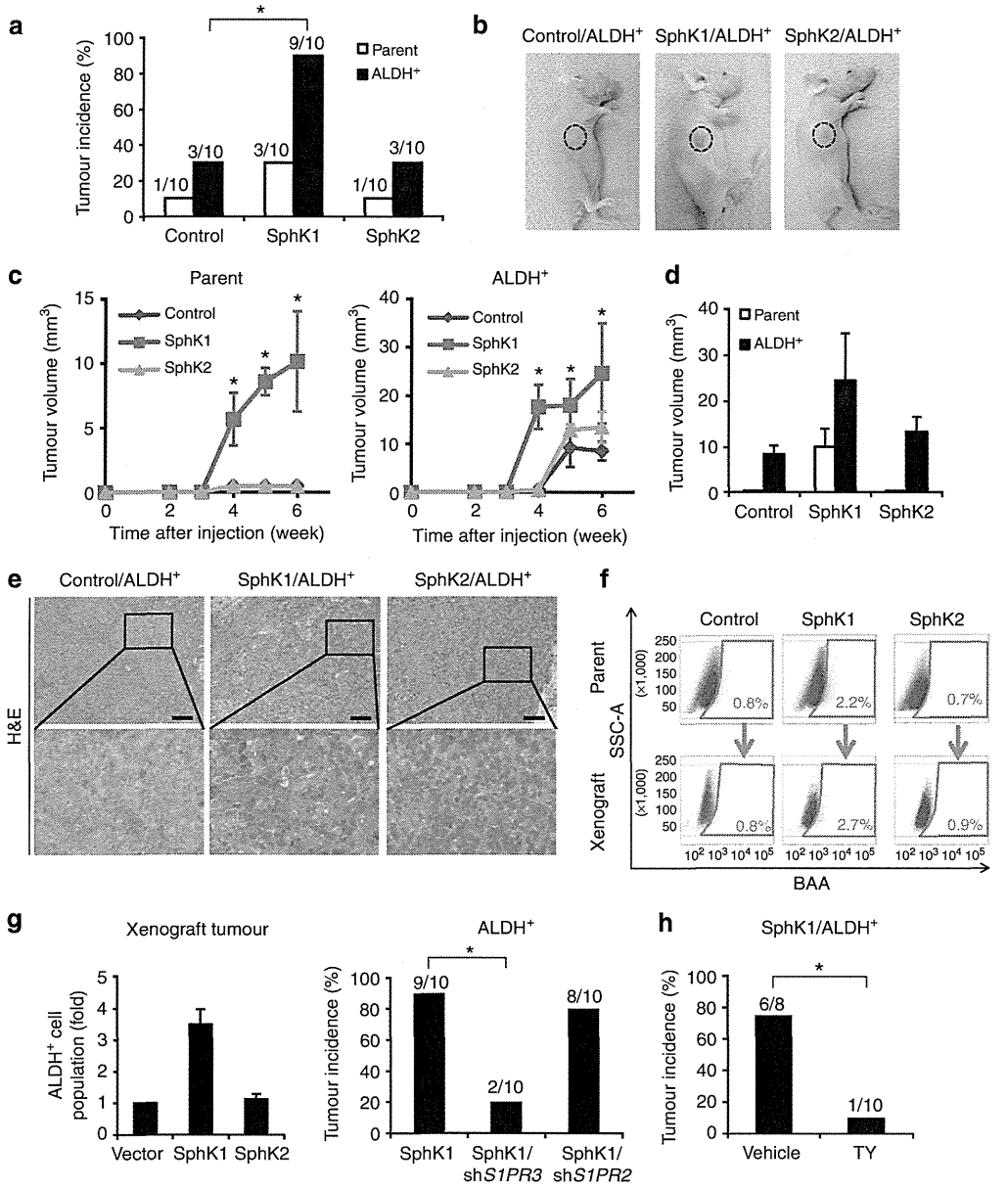

Figure 6 | SphK1 increases CSC-mediated tumour formation in a mouse xenograft model. (**a**) Balb/c nude mice were subcutaneously injected with 1×10^5 vector- or SphK-transfected MCF-7 cells. Tumour formation was indicated by tumours/injections at 6 weeks post injection. The *P* value was calculated using the Fisher's exact test. Bonferroni correction was applied for multiple comparisons. $^*P<0.05$ versus control. (**b**) Photographs of representative nude mice transplanted with ALDH-positive cells, SphK1-overexpressing ALDH-positive cells and SphK2-overexpressing ALDH-positive cells. (**c**) Tumour growth curves in the nude mice injected with parent or ALDH-positive cells. Tumour volume is presented as the mean ± s.d. ($n=10$). Kruskal–Wallis test, followed by the Steel–Dwass was used to determine significance. $^*P<0.05$ versus control. (**d**) Tumour volumes at 6 weeks post injection. Data represent mean ± s.d. ($n=10$). (**e**) Hematoxylin/eosin (H&E)-stained sections of tumour xenografts derived from vector-, SphK1-, and SphK2-overexpressing ALDH-positive cells. Scale bar, 100 μm. (**f**) Representative flow cytometry analysis of ALDH activity in the xenograft tumours derived from vector-, SphK1-, and SphK2-overexpressing ALDH-positive cells. The graph indicates ALDH-positive cell population in xenograft tumours. Data represent mean ± s.d. ($n=3$). ALDH-positive cells were able to regenerate the phenotypic heterogeneity in the xenograft tumours of nude mice. (**g**) Balb/c nude mice were subcutaneously injected with 1×10^5 vector-, *S1PR3*- or *S1PR2*-knockdown cells from SphK1-overexpressing ALDH-positive cells. Tumor formation was indicated by tumours/injections at 6 weeks post injection. The *P* value was calculated using the Fisher's exact test. Bonferroni correction was applied for multiple comparisons. $^*P<0.05$ versus control. (**h**) TY52156 or vehicle was inserted in subcutaneously implanted Alzet osmotic pumps before injection of 1×10^5 SphK1-overexpressing ALDH-positive cells. Tumour formation was indicated by tumours/injections at 6 weeks post injection. The *P* value was calculated using the Fisher's exact test. $^*P<0.05$ versus control.

We also identified S1P-induced Notch activation without Notch ligands. Consistent with our observations, previous studies have shown that ADAM17 mediates ligand-independent Notch activation, while ADAM10 is ligand dependent[38,39]. Another study has shown that soluble form of Jagged1 activates Notch signalling without cell–cell contact[40]. Furthermore, a recent study showed that multiple GPCRs, including the S1PR, resulted in shedding of TGFα via ADAM17 activation in HEK293 cells[41]. Within the S1PR family, S1PR3 has higher intrinsic activity for shedding. These data strongly support a signalling pathway

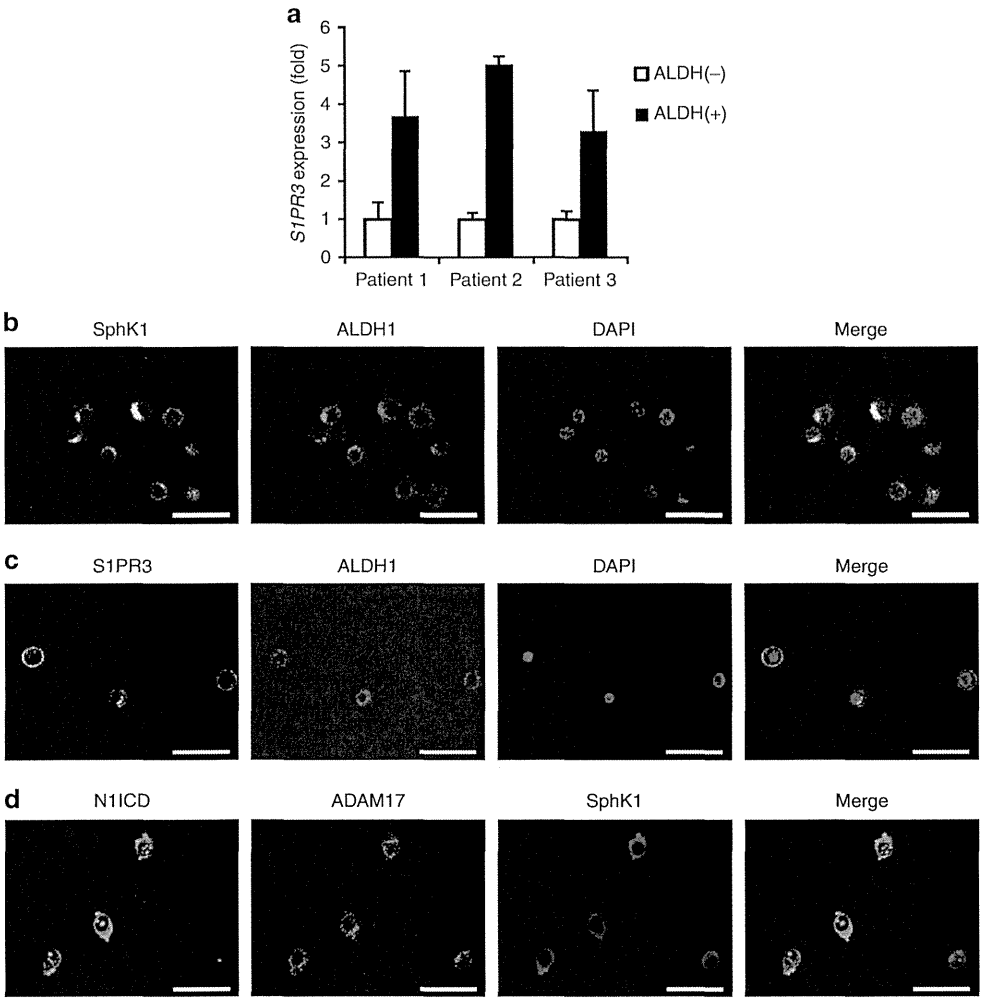

Figure 7 | SphK1-positive CSCs in human breast cancers. (**a**) *S1PR3* expression in the ALDH-negative or ALDH-positive patient-derived cells by qPCR. Expression levels were normalized to glyceraldehyde 3-phosphate dehydrogenase messenger RNAs. Data represent mean ± s.d. ($n=3$). (**b**) Double immunostaining of SphK1 (green) and ALDH1 (red) in patient-derived tumour cells. Nuclei were counterstained by DAPI (blue). (**c**) Double immunostaining of S1PR3 (green) and ALDH1 (red) in patient-derived tumour cells. Nuclei were counterstained by DAPI (blue). (**d**) Triple immunostaining of N1ICD (green), ADAM17 (red) and SphK1 (blue) in patient-derived tumour cells. Scale bar, 20 μm.

between the S1PR and ADAM17 activation in Notch ligands-independent manner. Further studies should be conducted looking at how the Notch system induces CSC phenotypes in breast cancer.

Our data demonstrate an essential cell autonomous role of Notch1 in breast CSCs expansion. Harrison *et al.*[42] has reported that Notch4 also affects breast CSCs. They performed knockdown of Notch paralog (Notch1 and Notch4) using both $ESA^+/CD44^+/CD24^{low}$ and mammosphere prepared from MCF-7 cells, although Notch ICD overexpression was not examined. Notch1 knockdown reduced only mammosphere population, whereas Notch4 knockdown reduced both $ESA^+/CD44^+/CD24^{low}$ and mammosphere populations (as shown in Figs 3a and 4b). Because Ginestier *et al.*[4] have already reported that two stem-like cell populations defined by ALDH positive and $CD44^+/CD24^-/lin^-$ were not identical, there is a possibility that discrepancy between our present data and Harrison's report is caused by the differences of cell populations used in the experiments. Thus, Notch paralog possibly plays a role in regulation in different stem cell population.

Our clinical samples suggest the crosstalk between Sphk1-S1P-S1PR3 and Notch signalling by co-localization of the components for the crosstalk machinery. Similar observations were obtained using xenografted tumour samples in nude mice. SphK1 has been already shown to be upregulated in patients with breast cancer[43], and its expression correlates with cancer progression and poor prognosis[43–45]. In addition, S1PR3 is the most highly expressed S1PR in breast cancer cells[46]. Thus, our data provide a potential explanation for significance of Sphk1-S1PR3-Notch axis in breast cancer.

Targeting Notch has been expected to facilitate tumour regression[47]. Although several types of Notch inhibitors are quite effective in preclinical models[21,48,49], none of the clinical trials conducted so far has examined effectiveness[50]. This prompts us to encourage efforts to explore alternative/additional approaches for targeting Notch. Our evidence suggests that Notch1 is involved in the S1P-induced CSC phenotype. Because lipid signalling acts upstream of the Notch, S1PR3 could be a promising target for various cancer. Indeed, TY52156 inhibited the tumorigenicity of SphK1-overexpressing breast CSCs (Fig. 6). Although several S1PR antagonists are currently available[14], few have been tested in clinical trials. The feasibility of S1PR3 antagonists in cancer remains to be determined.

In conclusion, the identification of S1P-derived CSC phenotype is required for continuous tumour growth, and points to potential

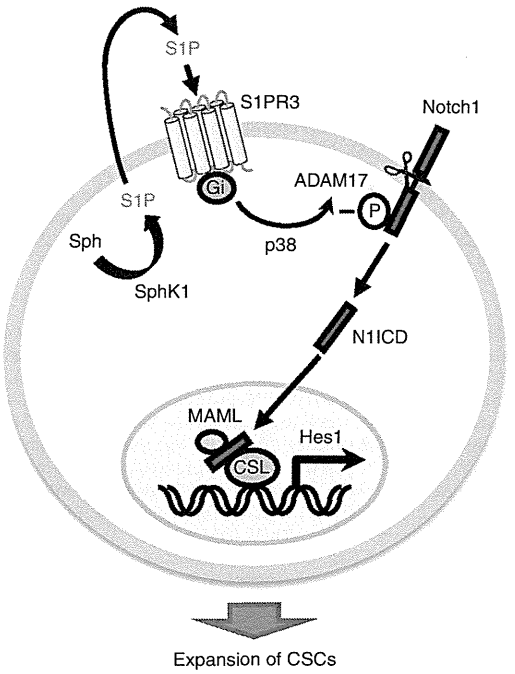

Figure 8 | A working model for the functions of SphK/S1P/S1PR3 in CSC regulation. S1P produced by SphK1 stimulates S1PR3 and subsequently activates Notch signaling in a Notch ligand-independent manner. Activation of S1P signaling pathway leads to expansion of CSCs.

culprits of tumour formation in patients. In the future, it might be possible to establish specific treatments that reduce tumorigenesis by targeting 'stemness' in cancer. Thus, efforts should be made to develop drugs capable of inhibiting CSC self-renewal and expansion by S1PR3.

Methods

Materials. Antibodies to p38MAPK (#9212), phospho-p38MAPK (#9211), Akt (#9272), phospho-Akt (#9271), Notch1 (#4380), N1ICD (#2421) and Notch3 (#2889) were from Cell Signaling Technology. Antibodies to HA (#H6908), FLAG (M2) (#F1804), myc (#C3956), β-actin (#A5441) and ADAM17 (phospho-Thr735) (#SAB4504073) were from Sigma-Aldrich. Antibody to ADAM17 (#AB19027) was from Millipore. Antibody to APC-conjugated TRA-1-85 (#FAB3195A) was from R&D Systems. Antibody to SphK1 (#AP7237c) was from Abgent. Antibody to ALDH1 (#611194), FITC mouse anti-human CD44 (#555478), PE mouse anti-human CD24 (#555428), FITC mouse IgG2b κ isotype control (#555742) and PE mouse IgG2a κ isotype control (#555574) were from BD Biosciences. Antibodies to S1PR2 (#sc-25491), S1PR3 (#sc-30024) and Spns2 (#130102) were from Santa Cruz Biotechnology. Antibody to SphK1 (#ab46719), ADAM17 (#ab57484), activated Notch1 (#ab8925) and ABCC1 (#ab3368) were from Abcam. Antibody to Alexa488-conjugated anti-rabbit IgG (#A11034) and Alexa555-conjugated anti-mouse IgG (#A21424) were from Invitrogen. S1P, dihydro-S1P, DAPT, SB203580, 5-Fluorouracil and doxorubicin were from Enzo Life Sciences. CAY10444, JTE013, MK571, LY294002, cyclopamine were from Cayman Chemicals. LPA was from Avanti Polar Lipids. Jagged1-Fc, Sonic hedgehog and Wnt3a were from R&D Systems. Botulinum C3 enzyme was from Bio Academia. PTX were from Wako Pure Chemical (Osaka, Japan). Hoechst, reserpine, DFO and PNU74654 were from Sigma-Aldrich, while N,N′-bis(4-chlorophenyl)-3,3-dimethyl-2-oxobutanehydrazonamide (TY52156) was synthesized. All other reagents were of analytical grade and obtained from commercial sources.

Cell culture. MCF-7 cells (American Type Culture Collection), MDA-MB-231 cells (American Type Culture Collection), A549 cells (European Collection of Cell Cultures) and LNCaP cells (European Collection of Cell Cultures), U251 cells (Japanese Collection of Research Biosources) were cultured in Dulbecco's modified Eagle's medium (DMEM; Sigma-Aldrich) supplemented with 10% heat-inactivated fetal bovine serum (FBS; Biological Industries), 100 U ml^{-1} penicillin and 100 μg ml^{-1} streptomycin (Gibco BRL). OVCAR-5 cells was cultured in RPMI1640 (Sigma-Aldrich) supplemented with 10% heat-inactivated FBS (Biological Industries), 100 U ml^{-1} penicillin and 100 μg ml^{-1} streptomycin (Gibco BRL).

Plasmid constructs and reporter assays. Plasmids encoding SphK1, SphK2, DN-CSL, DN-MAML, N1ICD, ADAM10 and 12xCSL-luc were kindly provided from Drs Stuart M. Pitson (University of Adelaide), Taro Okada (Kobe University), Aly Karsan (British Columbia Cancer Research Centre), Anthony J. Capobianco (University of Pennsylvania), Spyros Artavanis-Tsakonas (Harvard Medical School), Stefan Lichtenthaler (Ludvig Maximilians University) and Lothar J. Strobl (German Research Center for Environmental Health), respectively. Plasmids encoding N2ICD, N3ICD and N4ICD were kindly provided by Dr Michael J. Hendzel (University of Alberta). Plasmids encoding ADAM17 and DN-ADAM17 were kindly provided by Dr Rik Derynck (University of California, San Francisco). Plasmids encoding CA-G_i and CA-G_{12} were kindly provided by Dr J. Silvio Gutkind (National Institutes of Health). Plasmids encoding the ADAM17 mutants T735A and T761A were generated by QuikChange Site-Directed Mutagenesis (Stratagene) using pRK5-ADAM17-myc. A plasmid encoding the ADAM10 mutant E384A (DN-ADAM10) was generated by QuikChange Site-Directed Mutagenesis using peak-12-ADAM10-HA. Coding DNA sequences were verified by DNA sequencing. Transfections were conducted with FuGENE HD transfection reagent (Promega). Luciferase activity was assayed 24 h after transfection with 12xCSL-luc using the Glo Luciferase Assay Kit (Promega).

Microarray analysis. Total RNAs were isolated by Trizol (Invitrogen) and then purified using an RNeasy Mini Kit (Qiagen). Affymetrix Genome U133A gene chips (Affymetrix) were used to examine gene expression patterns according to the manufacturer's instruction. Genes upregulated more than twofold are shown in Supplementary Data 1.

ALDH assays. The ALDEFLUOR kit (Stem Cell Technologies) was used to detect CSC populations with high ALDH enzyme activity according to the manufacture's instruction[18]. The cells were plated at a density of 3×10^5 cells in 100 mm culture dishes. After serum deprivation for 3 days, cells were suspended at a concentration of 1×10^6 cells ml^{-1} in ALDH assay buffer containing the ALDH substrate BAAA (1 μM) and incubated for 30 min at 37 °C. As a negative control, cells were treated with diethylaminobenzaldehyde (15 μM), a specific ALDH inhibitor. A FACS Aria II cell sorter (BD Biosciences) was used to measure the ALDH-positive cell population.

Mammosphere-forming assays. MCF-7 cells were plated as single cells on ultralow attachment 6-well plates (Corning) at a concentration of 10,000 cells ml^{-1} in serum-free DMEM supplemented with N_2 supplement (Gibco) and 20 ng ml^{-1} basic Fibroblast Growth Factor (R&D Systems). After 4 days, the number of mammospheres was microscopically counted and the percentage of mammosphere-forming cells was determined as mammosphere-forming efficiency (%)[7].

SP assays. Cells were collected and suspended in prewarmed DMEM containing 2% FBS and 2 mM HEPES buffer. Hoechst 33342 dye (Sigma-Aldrich) was then added to a final concentration of 5 μg ml^{-1}, and the mixture was incubated with intermittent shaking for 60 min at 37 °C in the presence or absence of reserpine (15 μg ml^{-1}; Sigma-Aldrich). Cells were then resuspended in ice-cold phosphate-buffered saline (PBS) containing 2% FBS, and analysed with a FACS Aria II cell sorter (BD Biosciences).

CD44$^+$/CD24$^-$ cell population. Cells were resuspended in PBS containing 5% FBS and incubated with FITC mouse anti-human CD44 (#555478, 1:5) and PE mouse anti-human CD24 (#555428, 1:5) for 15 min at 4 °C. FITC mouse IgG2b κ isotype control (#555742, 1:5) and PE mouse IgG2a κ isotype control (#555574, 1:5) were used as negative control. Analysis was performed using a FACS Aria II cell sorter (BD Biosciences).

Cell viability assays. MCF-7 cells and sorted ALDH-positive cells were plated onto 96-well plates at a density of 5,000 cells well^{-1}. After overnight culture, cells were treated with 100 μM 5-Fluorouracil or 10 μM doxorubicin. After 72 h, MTS assays were performed, according to the manufacturer's instruction (Promega).

qPCR assays. Total RNA was isolated from MCF-7 cells using Trizol (Invitrogen), according to the manufacturer's instructions. The qPCR assays were conducted with the aid of a QuantiTect SYBR Green RT-PCR Kit (Qiagen) and an ABI PRISM 7900HT sequence detection system (Applied Biosystems). The relative changes in transcript levels for each sample were determined by normalizing to glyceraldehyde 3-phosphate dehydrogenase mRNA levels. Primer sequences used for qPCR analysis are shown in Supplementary Table 2.

Reverse transcription PCR analysis of S1PRs. Total RNA was isolated from MCF-7 cells using Trizol, according to the manufacturer's instructions. A Super-Script III Fast-Strand Synthesis System (Invitrogen) was used for reverse transcription synthesis of cDNAs. PCR amplification was performed with PrimeStar HS DNA polymerase (Takara) using GeneAmp PCR System 9700 (Applied

Biosystems). The cycling conditions were as follows: 1 min at 95 °C, 40 cycles of 30 s at 95 °C, 30 s at 54–66 °C, 1 min at 72 °C, following 7 min at 72 °C. Primer sequences used for reverse transcription PCR analysis are shown in Supplementary Table 2.

Transient RNA interference. Double-strand RNA oligonucleotides (siRNAs) against *S1PR3*, *S1PR2* and appropriate control scrambled siRNA were from Santa Cruz Biotechnology. The siRNAs against *Notch1*, *ABCC1* and *Spns2* were from Invitrogen. The siRNAs were transfected into MCF-7 cells using RNAiMax (Invitrogen) according to the manufacturer's recommendations.

Stable knockdown by lentiviral shRNA transduction. For stable gene silencing of *S1PR3* or *S1PR2*, specific shRNA MISSION lentiviruses (Sigma-Aldrich) were transduced into cells. The target sequence was 5′-CCGGGATCCTCTACGCAC GCATCTACTCGAGTAGATGCGTGCGTAGAGGATCTTTTTG-3′ for sh*S1PR3* and 5′-CCGGACTTTACCACCTGGTACAAAGCTCGAGCTTTGTACCAGGTG GTAAAGTTTTTTG-3′ for sh*S1PR2*. The transduced cells were selected in growth medium containing 1.5 μg ml^{-1} puromycin (Sigma-Aldrich).

Immunoblot analysis. Cells were lysed in Cell Lysis Buffer (Cell Signaling Technology) on ice for 30 min. Lysates were subjected to sodium dodecyl sulphate polyacrylamide gel electrophoresis and transferred to Immobilon-P Transfer Membrane (Millipore). Membranes were blocked with 5% (w/v) bovine serum albumin in Tris-buffered saline containing 0.1% Tween-20 (TBST) and incubated with primary antibodies overnight at 4 °C. Membranes were then incubated with horseradish peroxidase-conjugated secondary antibodies (Cell Signaling Technology, 1:2,000) for 1 h at room temperature and detected using ECL Prime Western Blotting Detection Reagent (GE Healthcare). Images were acquired using a LAS-3000 Imager (Fujifilm). The density of each band was quantified using an image analyser (Multi Gauge software, Fujifilm). The primary antibodies used were S1PR3 (#sc-30024, 1:2,000), S1PR2 (#sc-25491, 1:1,000), Notch1 (#4380, 1:1,000), N1ICD (#2421, 1:1,000), Notch3 (#2889, 1:1,000), FLAG (#F1804, 1:1,000), myc (#C3956, 1:5,000), HA (#H6908, 1:1,000), phospho-ADAM17 (#SAB4504073, 1:1,000), ADAM17 (#AB19027, 1:1,000), phospho-p38MAPK (#9211, 1:1,000), p38MAPK (#9212, 1:1,000), phospho-Akt (#9271, 1:1,000), Akt (#9272, 1:1,000), SphK1 (#AP7237c, 1:500), SphK2 (a gift from Dr T. Okada at Kobe University, 1:3,000), ABCC1 (#ab3368, 1:1,000), Spns2 (#sc-130102, 1:1,000) and β-actin (#A5441, 1:10,000). Original immunoblots are shown in Supplementary Fig. 19.

Immunocytochemistry. SphK-overexpressing MCF-7 cells and mammosphere cells were plated on glass coverslips. Cells were fixed with 4% paraformaldehyde and permeabilized with 0.2% Triton X-100. Coverslips were blocked with 5% FBS and incubated overnight at 4 °C with primary antibodies that recognized FLAG (#F1804, 1:500), HA (#H6908, 1:120), SphK1 (#ab46719, 1:50), S1PR3 (#sc-30024, 1:50), ALDH1 (#611194, 1:100). ADAM17 (#ab57484, 1:300) and activated Notch1 (#ab8925, 1:200). After rinsing with PBS, coverslips were incubated for 1 h at room temperature with Alexa488-conjugated (#A11034, 1:200) or Alexa555-conjugated (#A21424, 1:200) secondary antibody. In the case of triple staining of Sphk1, ALDH1 and N1ICD, antibody to SphK1 was labelled with AMCA conjugation kit (Abcam). After rinsing with PBS, coverslips were incubated with AMCA-conjugated SphK1 antibody (1:100) for 1.5 h. Nuclei were counterstained with DAPI (Nacalai Tesque). Fluorescence images were obtained using a Nikon A1 confocal microscope (Nikon).

Immunoprecipitation assay. Immunoprecipitation was conducted as previously reported with slight modifications[51]. MCF-7 cells were transfected with myc-tagged ADAM17. At 48 h after transfection, cells were lysed in lysis buffer (20 mM Tris-HCl pH 7.4, 200 mM NaCl, 0.1% NP-40, 10 mM NaF, 1 mM Na_3VO_4 and complete mini protease inhibitor cocktail (Roche Applied Sciences)). Lysates (100 μg) were incubated with myc-specific polyclonal antibody (#C3956, 1 μg) or normal rabbit IgG (#PM035, MBL, 1 μg) overnight at 4 °C. Subsequently, Protein G Sepharose (Amersham Pharmacia Biotech) was added to the mixture and incubated for an additional 2 h at 4 °C. Beads were washed with lysis buffer and immunoprecipitated proteins analysed by immunoblotting using a p38MAPK-specific polyclonal antibody (#9212) and a myc-specific polyclonal antibody (#C3956).

ADAM17 activity. ADAM17 activity was measured using a SensoLyte 520 ADAM17 Activity Assay Kit (ANASPEC) according to the manufacture's instruction[52]. MCF-7 cells were scraped in PBS containing a complete mini protease inhibitor cocktail and lysed using five cycles of freeze–thawing. Lysed cells were centrifuged at 20,000 *g* for 15 min and pelleted membranes resuspended with assay buffer. Approximately 15 μg of proteins were mixed with substrate for 30 min and fluorescence intensity was measured using a Wallac1420ARVO fluoroscan (Perkin Elmer), with excitation at 490 nm and emission at 520 nm.

γ-secretase activity. The activity of γ-secretase was measured using a specific fluorogenic substrate assay[53]. Cells were collected in cell lysis buffer containing (20 mM HEPES pH 7.0, 150 mM KCl, 2 mM EDTA, 1% (3-cholamidopropyl) dimethylammonio]-2-hydroxy-1-propanesulfonate (CHAPSO; Dojindo Laboratories), and complete Mini, EDTA-free protease inhibitor cocktail (Roche)). Lysates were centrifuged at 10,000 *g* for 1 min at 4 °C to remove nuclei and large cell debris. Approximately 5 μg of protein was added to each well of a white 96-well polystyrene microplate (Packard) and an equal volume of assay buffer (50 mM Tris–HCl (pH 6.8), 2 mM EDTA, and 0.25% (3-cholamidopropyl) dimethylammonio]-2-hydroxy-1-propanesulfonate (w/v)) added. 10 μM fluorogenic γ-secretase substrate (Peptide) was added to the plate and samples incubated at 37 °C for 4 h in the dark. Fluorescence intensity was measured using a Wallac1420ARVO fluoroscan (Perkin Elmer) with excitation at 355 nm and emission at 460 nm.

SphK activity. SphK activity was measured using omega-(7-nitro-2-1,3-benzoxadiazol-4-yl)-D-erythro-sphingosine-labelled fluorescent substrate[54]. Cells were lysed with a single freeze–thaw cycle in 50 mM HEPES (pH 7.4), 10 mM KCl, 15 mM $MgCl_2$, 0.1% Triton X-100, 20% glycerol, 2 mM orthovanadate, 2 mM dithiothreitol, 10 mM NaF, 1 mM deoxypyridoxine and complete Mini, EDTA-free protease inhibitor cocktail (Roche). The lysate was cleared by centrifuging at 20,000 *g* for 15 min at 4 °C. SphK1 activity was measured in 50 mM HEPES (pH 7.4), 15 mM $MgCl_2$, 0.5% Triton X-100, 10% glycerol, 5 mM NaF, 1 mM deoxypyridoxine, 2 mM ATP and 10 μM NBD-sphingosine (Avanti Polar Lipids). SphK2 activity was measured in 50 mM HEPES (pH 7.4), 15 mM $MgCl_2$, 0.5 M KCl, 10% glycerol, 5 mM NaF, 1 mM deoxypyridoxine, 2 mM ATP and 10 μM NBD- sphingosine. Reactions were started with the addition of 5 μg of lysate protein and incubated for 4 h at room temperature. Reactions were extracted with the addition of 1 M potassium phosphate (pH 8.5), followed by chloroform/methanol (2:1), then cleared at 15,000 *g* for 1 min. The upper aqueous layer was placed into the wells of white 96-well polystyrene microplates (Packard). Fluorescence intensity was measured with a Wallac1420ARVO fluoroscan (Perkin Elmer) with excitation at 485 nm and emission at 535 nm.

Tumorigenicity assay. The animal study protocol was reviewed and approved by the animal care and use committee of the institute. Six-week-old female Balb/c nude mice (CLEA Japan) were used in these studies and were given injections of 17-β-estradiol (Sigma-Aldrich) dissolved in pure sesame oil (0.1 mg 0.05 ml^{-1} sesame oil per mouse, subcutaneously) 1 day before tumour inoculation, and at weekly intervals, according to a previously reported protocol with slight modifications[55]. The ALDH-positive cell population was sorted by FACS (BD Aria II) and suspended in PBS mixed with an equal volume of Matrigel (BD Biosciences). Mice were given bilateral subcutaneous injections of 1×10^5 (0.1 ml) cells. Tumour growth was monitored for 6 weeks and analysed. Tumour volume was determined using the formula: $V = ½ \times \text{larger diameter} \times (\text{smaller diameter})^2$.

For the immunohistochemistry, paraffin-embedded sections of breast tumours from xenografts were deparaffinized in xylene and rehydrated in graded alcohol. Antigen retrieval was conducted three times by microwaving the slides in 0.01 M citrate buffer (pH 6.0) for 5 min. Sections were blocked with 5% FBS and incubated for 1.5 h with primary antibodies that recognized S1PR3 (#sc-30024, 1:50) and ALDH1 (#611194, 1:100). After rinsing with PBS, coverslips were incubated for 1 h at room temperature with Alexa488-conjugated (#A11034, 1:200) or Alexa555-conjugated (#A21424, 1:200) secondary antibody. Nuclei were counterstained with DAPI (Nacalai Tesque). Fluorescence images were obtained using a Biorevo BZ-9000 (Keyence). The number of S1PR3- and ALDH1 double-positive cells was counted in five fields[56].

For the hierarchy assay, the xenografts were collected after 6 weeks, dissociated into single cells and TRA-1-85-positive cells analysed using the ALDH assays[57]. Single cells were suspended in ALDH assay buffer containing the BAAA (1 μM) and incubated 30 min at 37 °C. The cells were resuspended in ALDH assay buffer for subsequent staining with the APC-conjugated TRA-1-85 antibody (#FAB3195A, 1:10), which recognizes human cells and thereby allows their discrimination from mouse cells. After incubation for 30 min and following centrifugation, the cells were resuspended in ALDH assay buffer containing 7-AAD (BD Bioscience, #559925) and analysed with a FACS Aria II cell sorter (BD Bioscience).

For the chronic administration, TY52156 (167 mg ml^{-1} in a 1:1 mixture of DMSO and PEG400) was inserted in subcutaneously implanted Alzet osmotic pumps (Cupertino), designed to release TY52156 continuously (at about 25 μg h^{-1}) for 6 weeks.

Mammosphere formation from primary cells. Mammosphere formation using primary cells (Celprogen) was performed[7,8]. The cells were plated as single cells in ultralow attachment dishes (Corning) at a density of 20,000 viable cells ml^{-1} in mammary epithelial growth medium for 7 days. To make secondary mammospheres, primary mammospheres were collected by gentle centrifugation (200*g*), dissociated enzymatically (10 min in 0.05% trypsin–EDTA) and mechanically (pipetting with yellow tips) into a single-cell suspension. The cells obtained from dissociation were then seeded in ultralow attachment dishes in mammary epithelial growth medium again.

Statistical analysis. Results are shown as mean ± s.d. For tumour incidence, the *P* value was calculated using the Fisher's exact test (Fig. 6a,g,h). Bonferroni correction was applied for multiple comparisons (Fig. 6a,g). For tumour volume, the *P* value was calculated using the Kruskal–Wallis test, followed by *post hoc* Steel–Dwass's multiple comparison test (Fig. 6c). Differences at $P<0.05$ were considered to be significant. Statistical analyses were performed using Excel 2010 with the add-in software.

References

1. Visvader, J. E. & Lindeman, G. J. Cancer stem cells in solid tumours: accumulating evidence and unresolved questions. *Nat. Rev. Cancer* **8,** 755–768 (2008).
2. Bonnet, D. & Dick, J. E. Human acute myeloid leukemia is organized as a hierarchy that originates from a primitive hematopoietic cell. *Nat. Med.* **3,** 730–737 (1997).
3. Al-Hajj, M. *et al.* Prospective identification of tumorigenic breast cancer cells. *Proc. Natl Acad. Sci. USA* **100,** 3983–3988 (2003).
4. Ginestier, C. *et al.* ALDH1 is a marker of normal and malignant human mammary stem cells and a predictor of poor clinical outcome. *Cell Stem Cell* **1,** 555–567 (2007).
5. Jiang, F. *et al.* Aldehyde dehydrogenase 1 is a tumour stem cell-associated marker in lung cancer. *Mol. Cancer Res.* **7,** 330–338 (2009).
6. van den Hogen, C. *et al.* High aldehyde dehydrogenase activity identifies tumour-initiating and metastasis-initiating cells in human prostate cancer. *Cancer Res.* **70,** 5163–5173 (2010).
7. Hinohara, K. *et al.* ErbB receptor tyrosine kinase/NF-κB signaling controls mammosphere formation in human breast cancer. *Proc. Natl Acad. Sci. USA* **109,** 6584–6589 (2012).
8. Dontu, G. *et al. In vitro* propagation and transcriptional profiling of human mammary stem/progenitor cells. *Genes Dev.* **17,** 1253–1270 (2003).
9. Takebe, N. & Ivy, S. P. Controversies in cancer stem cells: targeting embryonic signaling pathways. *Clin. Cancer Res.* **16,** 3106–3112 (2010).
10. Scheel, C. *et al.* Paracrine and autocrine signals induce and maintain mesenchymal and stem cell states in the breast. *Cell* **145,** 926–940 (2011).
11. Takabe, K., Paugh, S. W., Milstian, S. & Spiegel, S. 'Inside-out' signalling of sphingosine-1-phosphate: therapeutic targets. *Pharmacol. Rev.* **60,** 181–195 (2008).
12. Kohama, T. *et al.* Molecular cloning and functional characterization of murine sphingosine kinase. *J. Biol. Chem.* **273,** 23722–23728 (1998).
13. Liu, H. *et al.* Molecular cloning and functional characterization of a novel mammalian sphingosine kinase type 2 isoform. *J. Biol. Chem.* **275,** 19513–19520 (2000).
14. Pyne, N. J. & Pyne, S. Sphingosine 1 phosphate and cancer. *Nat. Rev. Cancer* **10,** 489–503 (2010).
15. Fyrst, H. & Saba, J. D. An update on sphingosine-1-phosphate and other sphingolipid mediators. *Nat. Chem. Biol.* **6,** 489–497 (2010).
16. Nagahashi, M. *et al.* Sphingosine-1-phosphate produced by sphingosine kinase 1 promotes breast cancer progression by stimulating angiogenesis and lymphangiogenesis. *Cancer Res.* **72,** 726–735 (2012).
17. Charafe-Jauffret, E. *et al.* Breast cancer cell lines contain functional cancer stem cells with metastatic capacity and a distinct molecular signature. *Cancer Res.* **69,** 1302–1313 (2009).
18. Hirata, N., Sekino, Y. & Kanda, Y. Nicotine increases cancer stem cell population in MCF-7 cells. *Biochem. Biophys. Res. Commun.* **403,** 138–143 (2010).
19. Long, J. S. *et al.* Sphingosine 1-phosphate receptor 4 uses HER2 (ERBB2) to regulate extracellular signal regulated kinase-1/2 in MDA-MB-453 breast cancer cells. *J. Biol. Chem.* **285,** 35957–35966 (2010).
20. Lin, C. I., Chen, C. N., Lin, P. W. & Lee, H. Sphingosine-1-phosphate regulates inflammation-related genes in human endothelial cells thorough S1P1 and S1P3. *Biochem. Biophys. Res. Commun.* **355,** 895–901 (2007).
21. Murakami, A. *et al.* Sphingosine 1-phosphate (S1P) regulates vascular contraction via S1P3 receptor: investigation based on a new S1P3 receptor antagonist. *Mol. Pharmacol.* **77,** 704–713 (2010).
22. Pannuti, A. *et al.* Targeting Notch to target cancer stem cells. *Clin. Cancer Res.* **16,** 3141–3152 (2010).
23. Noseda, M. *et al.* Smooth muscle α-actin is a direct target of Notch/CSL. *Circ. Res.* **98,** 1468–1470 (2006).
24. Jefflies, S., Robins, D. J. & Capobianco, A. J. Characterization of a high-molecular-weight Notch complex in the nucleus of Notch^{ic}-transformed RKE cells and in a human T-cell leukemia cell line. *Mol. Cell. Biol.* **22,** 3927–3941 (2002).
25. Artavanis-Tsakonas, S. & Muskavitch, M. A. Notch: the past, the present, and the future. *Curr. Top. Dev. Biol.* **92,** 1–29 (2010).
26. Ladi, E. *et al.* The divergent DSL ligand Dll3 does not activate Notch signaling but cell autonomously attenuates signaling induced by other DSL ligands. *J. Cell Biol.* **170,** 983–992 (2005).
27. Liu, C. *et al.* TACE-mediated ectodomain shedding of the type I TGF-β receptor downregulates TGF-β signaling. *Mol. Cell* **35,** 25–36 (2009).
28. Lammich, S. *et al.* Constitutive and regulated α-secretase cleavage of Alzheimer's amyloid precursor protein by a disintegrin metalloprotease. *Proc. Natl Acad. Sci. USA* **96,** 3922–3927 (1999).
29. Diaz-Rodriguez, E. *et al.* Extracellular signal-regulated kinase phosphorylates tumour necrosis factor alpha-converting enzyme at threonine 735: a potential role in regulated shedding. *Mol. Biol. Cell* **13,** 2031–2044 (2002).
30. Fan, H., Turck, C. W. & Derynck, R. Characterization of growth factor-induced serine phosphorylation of tumour necrosis factor-alpha converting enzyme and of an alternatively translated polypeptide. *J. Biol. Chem.* **278,** 18617–18627 (2003).
31. Xu, P. & Derynck, R. Direct activation of TACE-mediated ectodomain shedding by p38 MAP kinase regulates EGF receptor-dependent cell proliferation. *Mol. Cell* **37,** 551–566 (2010).
32. Pitson, S. M. *et al.* Phosphorylation-dependent translocation of sphingosine kinase to the plasma membrane drives its oncogenic signaling. *J. Exp. Med.* **201,** 49–54 (2005).
33. Igarashi, N. *et al.* Sphingosine kinase 2 is a nuclear protein and inhibits DNA synthesis. *J. Biol. Chem.* **278,** 46832–46839 (2003).
34. Takabe, K. *et al.* Estradiol induces export of sphingosine 1-phosphate from breast cancer cells via ABCC1 and ABCG2. *J. Biol. Chem.* **285,** 10477–10486 (2010).
35. Kawahara, A. *et al.* The sphingolipid transporter spns2 functions in migration of zebrafish myocardial precursors. *Science* **323,** 524–527 (2009).
36. Pébay, A. *et al.* Essential roles of sphingosine-1-phosphate and platelet-derived growth factor in the maintenance of human embryonic stem cells. *Stem Cells* **23,** 1541–1548 (2005).
37. Pitson, S. M. & Pébay, A. Regulation of stem cell pluripotency and neural differentiation by lysophospholipids. *Neurosignals* **17,** 242–254 (2009).
38. Bozkulak, E. C. & Weinmaster, G. Selective use of ADAM10 and ADAM17 in activation of Notch1 signaling. *Mol. Cell. Biol.* **29,** 5679–5695 (2009).
39. van Tetering, G. *et al.* Metalloprotease ADAM10 is required for Notch1 site 2 cleavage. *J. Biol. Chem.* **284,** 31018–31027 (2009).
40. Lu, J. *et al.* Endothelial cells promote the colorectal cancer stem cell phenotype through a soluble form of Jagged-1. *Cancer Cell* **23,** 171–185 (2013).
41. Inoue, A. *et al.* TGFα shedding assay: an accurate and versatile method for detecting GPCR activation. *Nat. Methods* **9,** 1021–1029 (2012).
42. Harrison, H. *et al.* Regulation of breast cancer stem cell activity by signaling through the Notch 4 receptor. *Cancer Res.* **70,** 709–718 (2010).
43. Ruckhäberle, E. *et al.* Microarray analysis of altered sphingolipid metabolism reveals prognostic significance of sphingosine kinase 1 in breast cancer. *Breast Cancer Res. Treat.* **112,** 41–52 (2008).
44. Watson, C. *et al.* High expression of sphingosine 1-phosphate receptors, S1P1 and S1P3, sphingosine kinase 1, and extracellular signal-regulated kinase-1/2 is associated with development of tamoxifen resistance in estrogen receptor-positive breast cancer patients. *Am. J. Pathol.* **177,** 2205–2215 (2010).
45. Long, J. S. *et al.* Sphingosine kinase 1 induces tolerance to human epidermal growth factor receptor 2 and prevents formation of a migratory phenotype in response to sphingosine 1-phosphate in estrogen receptor-positive breast cancer cells. *Mol. Cell. Biol.* **30,** 3827–3841 (2010).
46. Goetzl, E. J. *et al.* Dual mechanisms for lysophospholipid induction of proliferation of human breast carcinoma cells. *Cancer Res.* **59,** 4732–4737 (1999).
47. Ranganathan, P., Weaver, K. L. & Capobianco, A. J. Notch signaling in solid tumours: a little bit of everything but not all the time. *Nat. Rev. Cancer* **11,** 338–351 (2011).
48. Debeb, B. G. *et al.* Pre-clinical studies of Notch signaling inhibitor RO4929097 in inflammatory breast cancer cells. *Breast Cancer Res. Treat.* **134,** 495–510 (2012).
49. Ramakrishnan, V. *et al.* MRK003, a γ-secretase inhibitor exhibits promising *in vitro* pre-clinical activity in multiple myeloma and non-Hodgkin's lymphoma. *Leukemia* **26,** 340–348 (2012).
50. Olsauskas-Kuprys, R., Zlobin, A. & Osipo, C. Gamma secretase inhibitors of Notch signaling. *OncoTargets Ther.* **6,** 943–955 (2013).
51. Kanda, Y., Mizuno, K., Kuroki, Y. & Watanabe, Y. Thrombin-induced p38 mitogen-activated protein kinase activation is mediated by epidermal growth factor receptor transactivation pathway. *Br. J. Pharmacol.* **132,** 1657–1664 (2001).
52. Rao, S., Liu, X., Freedman, B. D. & Behrens, E. M. Spleen tyrosine kinase (Syk)-dependent calcium signals mediate efficient CpG-induced exocytosis of tumour necrosis factor α (TNFα) in innate immune cells. *J. Biol. Chem.* **288,** 12448–12458 (2013).
53. Farmery, M. R. *et al.* Partial purification and characterization of gamma-secretase from post-mortem human brain. *J. Biol. Chem.* **278,** 24277–24284 (2003).

54. Don, A. S. *et al.* Essential requirement for sphingosine kinase 2 in a sphongolipid apoptosis pathway activated by FTY720 analogues. *J. Biol. Chem.* **282,** 15833–15842 (2007).
55. Zhou, J. *et al.* Activation of the PTEN/mTOR/STAT3 pathway in breast cancer stem-like cells is required for viability and maintenance. *Proc. Natl Acad. Sci. USA* **104,** 16158–16163 (2007).
56. Ahn, G. & Brown, J. M. Matrix metalloproteinase-9 is required for tumour vasculogenesis but not for angiogenesis: role of bone marrow-derived myelomonocytic cells. *Cancer Cell* **13,** 193–205 (2008).
57. Prasmickaite, L. *et al.* Aldehyde dehydrogenase (ALDH) activity does not select for cells with enhanced aggressive properties in malignant melanoma. *PLoS ONE* **5,** e10731 (2010).

Acknowledgements

We thank Dr Taro Okada for his helpful comments on the manuscript. We thank Stuart M. Pitson (University of Adelaide), Taro Okada (Kobe University), Aly Karsan (British Columbia Cancer Research Centre), Anthony J. Capobianco (University of Pennsylvania), Spyros Artavanis-Tsakonas (Harvard Medical School), Stefan Lichtenthaler (Ludvig Maximilians University), Lothar J. Strobl (German Research Center for Environmental Health), Michael J. Hendzel (University of Alberta), Rik Derynck (University of California, San Francisco), and J. Silvio Gutkind (National Institutes of Health) for providing the plasmids. We thank Dr Junya Kanda (Jichi Medical University) for assistance with statistical analyses. We also thank additional members of the laboratory and other members of the Institute for their advice and discussion. This work was supported by the Advanced research for medical products Mining Programme of the National Institute of Biomedical Innovation (NIBIO, #09-02 to Y.K.), a Grant-in-Aid for Scientific Research from the Ministry of Education, Culture, Sports, Science, and Technology, Japan (#23590322, #26670041 to Y.K.), a Health and Labour Sciences Research Grant from the Ministry of Health, Labour and Welfare, Japan (Y.K.), and a grant from the Smoking Research Foundation (Y.K.).

Author contributions

N.H. performed most of the experiments. Y.K. planned the project. Y.K. and Y.S. wrote the manuscript. S.Y. performed the experiments related to ADAM17 mutants. T.S. and M.K. performed the experiments related to TY52156. All authors participated in the preparation of the manuscript.

Additional information

Accession codes: Microarray data have been deposited in the NCBI Gene Expression Omnibus database under accession codes GSE59653.

Supplementary Information accompanies this paper at http://www.nature.com/naturecommunications

Competing financial interests: The authors declare no competing financial interests.

Reprints and permission information is available online at http://npg.nature.com/reprintsandpermissions/

How to cite this article: Hirata, N. *et al.* Sphingosine-1 phosphate promotes expansion of cancer stem cells via S1PR3 by a ligand-independent Notch activation. *Nat. Commun.* 5:4806 doi: 10.1038/ncomms5806 (2014).

Journal of Neurochemistry

JOURNAL OF NEUROCHEMISTRY | 2014 | 128 | 507–522 doi: 10.1111/jnc.12486

ORIGINAL ARTICLE

Spikar, a novel drebrin-binding protein, regulates the formation and stabilization of dendritic spines

Hiroyuki Yamazaki,* Nobuhiko Kojima,* Kenichi Kato,* Eiji Hirose,† Toshiharu Iwasaki,‡ Toshiyuki Mizui,* Hideto Takahashi,*,[1] Kenji Hanamura,* Reiko T. Roppongi,* Noriyuki Koibuchi,‡ Yuko Sekino,*,§ Nozomu Mori†,[2] and Tomoaki Shirao*

*Department of Neurobiology and Behavior, Gunma University Graduate School of Medicine, Maebashi, Japan

†National Center for Geriatrics and Gerontology, Obu, Japan

‡Integrative Physiology, Gunma University Graduate School of Medicine, Maebashi, Japan

§Division of Pharmacology, National Institute of Health Sciences, Tokyo, Japan

Abstract

Dendritic spines are small, actin-rich protrusions on dendrites, the development of which is fundamental for the formation of neural circuits. The actin cytoskeleton is central to dendritic spine morphogenesis. Drebrin is an actin-binding protein that is thought to initiate spine formation through a unique drebrin-actin complex at postsynaptic sites. However drebrin overexpression in neurons does not increase the final density of dendritic spines. In this study, we have identified and characterized a novel drebrin-binding protein, spikar. Spikar is localized in cell nuclei and dendritic spines, and accumulation of spikar in dendritic spines directly correlates with spine density. A reporter gene assay demonstrated that spikar acts as a transcriptional co-activator for nuclear receptors. We found that dendritic spine, but not nuclear, localization of spikar requires drebrin. RNA-interference knockdown and overexpression experiments demonstrated that extranuclear spikar regulates dendritic spine density by modulating *de novo* spine formation and retraction of existing spines. Unlike drebrin, spikar does not affect either the morphology or function of dendritic spines. These findings indicate that drebrin-mediated postsynaptic accumulation of spikar regulates spine density, but is not involved in regulation of spine morphology.

Keywords: dendritic spine, drebrin-binding protein, spine formation, transcriptional co-activator.

J. Neurochem. (2014) **128**, 507–522.

*Read the **Editorial Highlight** for this article on page 473.*

Neurons have numerous small, actin-rich protrusions called dendritic spines that receive the majority of excitatory inputs (Sala *et al.* 2008; Rochefort and Konnerth 2012). The formation of dendritic spines plays a pivotal role in the incorporation of neurons into neural circuits (Kwon and Sabatini 2011). It is widely accepted that dendritic filopodia are the precursors of dendritic spines and that the actin cytoskeleton is a central player in the morphological changes underlying dendritic spine formation (Ethell and Pasquale 2005; Sekino *et al.* 2007; Shirao and Gonzalez-Billault 2013).

Drebrin is an actin-binding protein that has been extensively studied. Drebrin bridges two actin protomers (Grintsevich *et al.* 2010) and induces structural and

Received July 25, 2013; revised manuscript received October 9, 2013; accepted October 10, 2013.

Address correspondence and reprint requests to Tomoaki Shirao, Department of Neurobiology and Behavior, Gunma University Graduate School of Medicine, 3-39-22 Showa-machi, Maebashi 371-8511, Japan. E-mail: tshirao@med.gunma-u.ac.jp.

[1]Present address: Institut de recherches cliniques de Montreal, Montreal, QC, Canada, H2W 1R7. [2]Present address: Department of Anatomy and Neurobiology, Nagasaki University School of Medicine, Nagasaki, Nagasaki 852-8523, Japan.

Abbreviations used: ADF-H domain, actin-depolymerizing factor homology domain; BSA, bovine serum albumin; DIV, days *in vitro*; DMEM, Dulbecco's modified Eagle medium; drebrinR, RNAi-resistant drebrin; ERα, estrogen receptor α; GR, glucocorticoid receptor; His^6-drebrin, His^6-tagged drebrin A; KD, knockdown; LUC, luciferase; mDsRED, monomeric DsRED; MEM, minimum essential medium; mEPSCs, miniature excitatory postsynaptic currents; mNLS, mutated NLS; NLS, nuclear localization sequence; PBS, phosphate-buffered saline; RNAi, RNA interference; spikar^R, RNAi-resistant spikar; T3, 3,3′,5-triiodo-L-thyronine; TRE, thyroid hormone response element; TRβ1, thyroid hormone receptor β1.

mechanical remodeling of *F*-actin that includes significant changes in filament helical twisting and stiffness (Sharma *et al.* 2011, 2012). Within cultured cells, overexpressed drebrin binds to *F*-actin (Shirao *et al.* 1988; Ishikawa *et al.* 1994) to form unique *F*-actin bundles that are different from those observed in stress fibers or lamellipodia (Shirao *et al.* 1994). Formation of a drebrin-actin complex at postsynaptic sites during development facilitates dendritic spine formation (Takahashi *et al.* 2003; Aoki *et al.* 2005). Drebrin knockdown decreases spine and filopodia densities (Takahashi *et al.* 2006) and the density of excitatory synapses (Ivanov *et al.* 2009). However, drebrin overexpression does not increase the number of normal spines (Hayashi and Shirao 1999; Mizui *et al.* 2005), even though it causes morphological changes in dendritic spines (Hayashi and Shirao 1999; Biou *et al.* 2008). These results indicate that drebrin initiates spine formation, but an increased amount of drebrin does not directly correlate with the final density of dendritic spines.

We postulated the existence of a novel drebrin-binding protein that plays a critical role in regulating spine density through changes in its expression level. Although drebrin forms a complex with actin, myosin, and gelsolin (Hayashi *et al.* 1996) as well as other drebrin-binding proteins such as Homer2 (Shiraishi *et al.* 2004) and profilin (Mammoto *et al.* 1998), spine density does not vary in direct proportion to the expression level of these molecules (Sala *et al.* 2003; Ryu *et al.* 2006; Gorlich *et al.* 2012). To identify a drebrin-binding molecule directly related to spine density, we performed a yeast two-hybrid screen using drebrin as bait. Based on the screen results, we isolated a novel drebrin-binding protein that we termed spikar (for **spi**ne and **kar**yoplasm protein). Knockdown and overexpression experiments performed with spikar indicated that its expression level parallels the density of dendritic spines.

Methods

Animals

All experiments were carried out in accordance with the guidelines of the Animal Care and Experimentation Committee, Gunma University, Showa Campus (Maebashi, Japan). Wistar rats were purchased from Japan SLC Inc. (Hamamatsu, Japan) and Charles River Laboratories Japan Inc. (Yokohama, Japan). Every effort was made to minimize animal suffering and reduce the number of animals used. Animals were kept in the animal house under standard white cyclic lighting, with free access to food and water.

Yeast two-hybrid system

The *Saccharomyces cerevisiae* transformation and two-hybrid screen were carried out using the Y190 strain. The N-terminal region of rat drebrin (corresponding to amino acid residues 1–233) was subcloned into the pAS404 vector, which was derived from pAS1 (Sekiguchi *et al.* 2001). Y190 cells were transformed with the bait plasmid pAS404-drebrin (1–233), using the conventional lithium acetate-polyethylene glycol method. The cells were grown on SD medium lacking tryptophan and further characterized by testing for protein expression and self-activation of the bait before screening. Large-scale transformation was performed using a rat brain cDNA library constructed in a pACT2 vector (Clontech, Palo Alto, CA, USA), and the cells were grown on SD medium lacking tryptophan, leucine, and histidine, and containing 25 mM 3-aminotriazole. The cells were subsequently assayed for activation of the HIS3 genes.

Molecular cloning of spikar cDNA

The rat spikar clone isolated from the two-hybrid screen lacked a 5′-coding sequence; therefore, the full-length cDNA was generated using a PCR-based strategy. To obtain the 5′ end of rat spikar cDNA, we performed 5′-rapid amplification of cDNA ends (RACE) using rat hippocampal cDNA and a 5′-Full RACE Core Set (Takara, Otsu, Japan).

Expression vectors

All spikar and drebrin constructs were generated by PCR using Pfu turbo DNA polymerase (Stratagene, La Jolla, CA, USA). Full-length spikar and its deletion mutants were subcloned into pEGFP-C1 (EGFP, enhanced green fluorescent protein) (Clontech), pCMV-Myc (Clontech) or pNN265-HA (Kojima *et al.* 1997). To generate the nuclear localization signal (NLS) mutant of spikar (mNLS-spikar), K44T and K45T mutations were introduced by PCR using the following primers: 5′-gccccattaaaacgacaaagaaacccggc-3′ and 5′-gccgggtttctttgtcgttttaatggggc-3′.monomeric DsRED-drebrin A was constructed by subcloning a rat drebrin A fragment into the pDsRed-Monomer-C1 (Clontech).

Reporter gene assays

The method of reporter gene assay has been described previously (Takeshita *et al.* 1998; Iwasaki *et al.* 2001, 2002). The details are provided in the Appendix S1.

In vitro binding assay

A binding assay for full-length drebrin and full-length spikar was performed using green fluorescent protein (GFP)-spikar and His^6-tagged drebrin A (His^6-drebrin). The His^6-drebrin construct was a gift from Dr Ishikawa (Ishikawa *et al.* 2007). His^6-drebrin was affinity purified using Ni-NTA Magnetic Agarose Beads (Qiagen, Hilden, Germany). Ni-NTA beads conjugated with His^6-drebrin were incubated with cell lysate expressing GFP-spikar for 2 h at 25°C. Following extensive washes with lysis buffer (20 mM Tris-HCl, pH 7.5, 150 mM NaCl, 1% NP40, 50 μg/mL DNase, 10 μg/mL RNase, 1 mM phenylmethanesulfonyl fluoride, 1 μg/mL leupeptin, and 1 μg/mL pepstatin), the Ni-NTA bead pellets were re-suspended in sodium dodecyl sulfate (SDS) sample buffer and analyzed by western blotting. For GST pull-down assay, Glutathione S-transferase (GST)-drebrin (1–138) (pGEX-4T-1, GE Health Care, Buckinghamshire, England) was purified directly from bacterial extracts on glutathione-Sepharose-4B (GE Health Care). Immobilized GST or GST-drebrin (1–138) fusion proteins were incubated with cell lysate expressing HA-spikar fragments (1–376, 377–1208, or 1–1208) for 2 h at 25°C. After extensive washes with lysis buffer, the GST bead pellets were re-suspended in SDS sample buffer and analyzed by western blotting.

Immunocytochemistry and immunohistochemistry

Cultured neurons were fixed in 4% paraformaldehyde at 4°C for 20 min. The fixed neurons were permeabilized with 0.1% Triton X-100 in phosphate-buffered saline (PBS) for 5 min and blocked with 3% bovine serum albumin (BSA) in PBS for 60 min. Primary antibodies were applied in 3% BSA/PBS at 4°C for 12 h. After washing with PBS three times for 5 min each, the appropriate secondary antibodies conjugated to fluorescein isothiocyanate, Cy5, or rhodamine (Chemicon, Temecula, CA, USA) were added and incubated for 1 h at 20–25°C.

Deeply anesthetized 7-week-old male Wistar rats were perfused intracardially with a fixative of 4% paraformaldehyde in 0.1 M phosphate buffer (pH 7.4). Brain tissue was post-fixed in the same fixative for 12 h and then equilibrated with 30% sucrose in PBS at 4°C. Frozen sections (25 μm) were cut on a cryostat and treated with 0.1% Triton X-100 in PBS for 10 min and then incubated with 3% BSA/PBS for 1 h. They were then incubated with the primary antibody for 12 h at 4°C, washed with PBS four times for 5 min each, incubated with a biotinylated secondary antibody (Vector Laboratories, Burlingame, CA, USA) for 1 h at 20–25°C, and washed four times for 5 min each. Visualization was performed with 3,3′-diaminobenzidine using the ABC method (Vectastain Elite kit, Vector Laboratories).

Western blot analysis and subcellular fractionation

Wistar rats were sacrificed after being deeply anesthetized, and various tissues were dissected and homogenized. Protein amounts were normalized to the wet weights of the original tissue samples. For subcellular fractionation, the cerebral cortices of seven adult male Wistar rats were homogenized in a buffered solution (320 mM sucrose, 4 mM HEPES-NaOH, pH 7.4) containing a protease inhibitor cocktail (Complete, Roche, Basel, Switzerland) and fractionated according to the method of Huttner *et al.* (1983). For extraction experiments, the P3 pellet was homogenized by a Teflon homogenizer in a buffer solution containing 1 M NaCl or 1% Triton X-100 and centrifuged at 165 000 *g*. The samples were denatured and subjected to SDS–polyacrylamide gel electrophoresis. The proteins were then transferred onto an Immobilon Transfer Membrane (Millipore, Bedford, MA, USA) and processed for immunodetection.

Antibodies

The following primary antibodies were used: mouse monoclonal anti-drebrin (M2F6; Shirao and Obata 1986), mouse monoclonal anti-PSD-95 (7E3-1B8; Affinity BioReagents, Golden, CO, USA), mouse monoclonal anti-MAP2 (HM-2; Sigma, St. Louis, MO, USA), mouse monoclonal anti-Glial fibrillary acidic protein (anti-GFAP) (G-A-5; Sigma) and rabbit polyclonal anti-synapsin I (Chemicon). Polyclonal anti-spikar antibodies were raised against the C-terminal region of spikar (377–1208). The DNA fragment of spikar (377–1208) was subcloned into pET19b (Novagen, Madison, WI, USA). His^6-spikar (377–1208) was affinity-purified using a Ni^{2+} column (GE Health Care) according to the manufacturer's instructions. This His^6-spikar (377–1208) protein (2 mg) was used to immunize rabbits. The specificity of the anti-spikar antibodies was confirmed by western blotting (Figure S1).

Cell culture and transfection

Hippocampi were dissected from the fetuses of timed pregnant Wistar rats at embryonic day 18. The hippocampi were trypsinized and dissociated by trituration according to methods described previously (Takahashi *et al.* 2003). Briefly, cell suspensions were plated at a density of 5000 cells/cm^2 on coverslips coated with poly-L-lysine and incubated in minimum essential medium (Invitrogen) supplemented with 10% fetal bovine serum. Following cell attachment, the coverslips were transferred to a culture dish containing a glial monolayer sheet and maintained in serum-free minimum essential medium with B27 supplement (Invitrogen). Cytosine β-D-arabinofuranoside (10 μM; Sigma) was added to the cultures at 4 days *in vitro* (DIV) to inhibit glial proliferation.

Cells were transfected using the CaPO4 method (Details are provided in Figure S2). Microinjection was performed using a micromanipulator 5171 (Eppendorf, Hamburg, Germany).

HEK293 cells were cultured in Dulbecco's modified Eagle medium supplemented with 10% fetal bovine serum at 37°C in a 5% CO_2 atmosphere. Cells were transfected using Lipofectamine 2000 (Invitrogen).

RNA interference

To generate the RNA interference (RNAi) constructs used in this study, the following DNA oligonucleotides were annealed and subcloned into the pSUPERneo+GFP vector (OligoEngine, Seattle, WA, USA): 5′-gatccccggatcagttagagttaggattcaagagatcttagctctgactg atccttttggaaa-3′ and 5′-agcttttccaaaaaggatcagtcagagctaagatctcttgaatc ctaactctaactgatccggg-3′ (Spikar-shRNA-2); 5′-gatccccgttgatgcaagtag cagagttcaagagactttgctatttgcgtcaacttttggaaa-3′ and 5′-agcttttccaaaaagt tgacgcaaatagcaaagtctcttgaactctgctacttgcatcaacggg-3′ (Spikar-shRNA -3); 5′-gatccccgtgatgtgtggtttctgtattcaagagatgcagaaaccgtacatcac tttttg gaaa-3′ and 5′-agcttttccaaaaagtgatgtacggtttctgcatctcttgaata cagaaacc acacatcacggg-3′ (Drebrin-shRNA); 5′-gatccccctacgttgagtacttcggttca agagatcgaagtactcagcgtaagttttta-3′ and 5′-agcttaaaaac ttacgctgagtact tcgatctcttgaaccgaagtactcaacgtaagggg3′ (Luciferase-shRNA). The targeted regions were not homologous to any other known genes, as confirmed by a BLAST search. The RNAi-resistant mutant of spikar-shRNA-3 was constructed by PCR using the following primers: 5′-ccacaagttgacgcagatcgcaaaggttgtcatc-3′ and 5′-gat-gacaaccctttgcgatctgcgtcaacttgtgg-3′. The RNAi-resistant mutant of drebrin was constructed by PCR using the following primers: 5′-gaaagtgatgtatggcttctgcagcgtc-3′ and 5′- gacgctgcagaagccatacatca ctttc-3′. A spikar-shRNA-3 construct was used to silence spikar. Cultured hippocampal neurons were transfected at 3 DIV with spikar-shRNA-3 to ensure that spikar expression would be suppressed during stage 5 of neuronal development (Dotti *et al.* 1988). Empty shRNA vector (pSUPERneo+GFP) was used as a control. The effect of the control vector on dendritic protrusions was similar to that of luciferase-shRNA vector (Figure S2). Another effective construct, spikar-shRNA-2, showed a reduction of the density of dendritic spines and filopodia similar to spikar-shRNA-3 (Figure S2). The efficiency of the drebrin knockdown construct has been described previously (Kato *et al.* 2012).

Electrophysiology

Whole-cell patch clamp recordings were performed with an Axopatch 200A amplifier (Axon Instruments, Union City, CA, USA) at 20–25°C. GFP-positive cultured hippocampal neurons from

17–19 DIV were identified using fluorescence microscopy (Olympus IX70, Tokyo, Japan) and used for electrophysiological studies. Patch pipettes were made from borosilicate glass capillaries (1.5 mm OD; Narishige, Tokyo, Japan) using a micropipette puller (P-87; Sutter Instrument, Novato, CA, USA). The resistance of the patch pipettes was 3–4 MΩ when filled with the pipette solution described below. The series resistance, 9.8 ± 0.6 MΩ, was not electronically compensated. The reference electrode was an Ag/AgCl electrode connected to the bath via an agar bridge filled with 150 mM NaCl. The potential of the pipette was corrected for the measured liquid junction potential (approximately 10 mV). Modified Tyrode solution was used as the external solution containing (in mM) 145 NaCl, 5 KCl, 2 $CaCl_2$, 1 $MgCl_2$, 10 glucose, and 10 HEPES (pH 7.4 with NaOH) plus 1 μM tetrodotoxin and 100 μM picrotoxin. The pipette solution contained (in mM) 122.5 Cs-gluconate, 17.5 CsCl, 8 NaCl, 0.2 EGTA, 2 ATP-Mg, 0.3 GTP, and 10 HEPES, and the pH was adjusted to 7.2 with Cs-OH. Whole-cell currents were recorded at 10 kHz after low-pass filtering at 2 kHz, and miniature excitatory postsynaptic currents (mEPSCs) were analyzed offline using Mini Analysis Software (Synaptosoft Inc., Decatur, GA, USA). We held the membrane potential of cultured neurons at −60 mV in voltage clamp and recorded the synaptic current.

Image analysis and statistics

Fluorescence images were acquired using a Zeiss Axioplan 2 microscope (Carl Zeiss, Jena, Germany) equipped with a CoolSnap fx CCD camera (Photometrics, Tucson, AZ, USA) and a 63 × oil-immersion, 1.4 NA (Carl Zeiss) objective at 25°C. The data were collected from two to three independent culture preparations, and analysis was performed by an experimenter blinded to the identity of the transfected constructs. Morphometric analysis and quantification were carried out using MetaMorph image analysis software (Molecular Devices, Sunnyvale, CA, USA). Neurons expressing GFP were imaged and quantified, and aspiny interneurons were excluded from the analysis. For each neuron, one or two dendrites 40–80 μm from the first branching point were selected and analyzed. For the morphological analysis of the dendritic protrusions, the maximum length and width of each protrusion of length 0.5–8 μm were measured manually (Figure S3a and b). Dendritic spines were defined as dendritic protrusions with a head or stubby type protrusion for which the length:width ratio was less than or equal to 2. Dendritic filopodia were defined as headless dendritic protrusions for which the length:width ratio was greater than 2. For the quantification of cluster number, clusters were defined as an immunostained region with a peak fluorescence level that was 2-fold greater than the averaged fluorescence level of the dendrites. For image analysis, statistical significance was determined with a Welch's *t*-test, Mann–Whitney U-test, Dunnett multiple comparison test, Tukey–Kramer multiple comparison test or Steel–Dwass multiple comparison test. Spine length and width were analyzed with the Kolmogorov–Smirnov test using SPSS software (SPSS, Chicago, IL, USA). *p* values less than 0.01 were considered statistically significant unless explicitly stated otherwise. For electrophysiology, statistical significance was determined with a Welch's *t*-test. Cumulative frequencies of mEPSC amplitude and inter-event interval were analyzed with the Kolmogorov–Smirnov test using Mini Analysis Software (Synaptosoft, Inc., NJ, USA). For reporter gene assays, all transfection studies were repeated at least twice in triplicate. Statistical analysis was performed using ANOVA followed by a post hoc comparison with Bonferroni's multiple range test. The data shown represent the mean values of triplicate transfections ± SEM.

Live-cell imaging

Live neurons were mounted in a modified 35-mm dish and imaged with a 40 × , 0.75 NA water-immersion objective (Carl Zeiss) in culture medium using the microscope described above. The images were captured within 5 min at 30°C.

Results

Spikar is a novel drebrin-binding transcriptional co-activator

To identify proteins that interact with drebrin, we performed a yeast two-hybrid screen using a rat brain cDNA library. We used the N-terminal region of drebrin (amino acids 1–233), which contains the actin-depolymerizing factor homology domain (ADF-H domain), as the screen bait. In the course of screening approximately 9×10^7 colonies, we isolated 89 independent clones. DNA sequencing of these clones showed that 64 of the 89 clones encoded the same protein. We termed this protein spikar (accession number AB074010); this name was derived from its unique subcellular localization (in spines and nuclei), as described in the following section. A computational analysis using the NCBI database indicated that spikar was a rat ortholog of human KIAA1125 (accession number AB032951) and human prkcbp1 (accession number AF233453) (Fossey *et al.* 2000), and that rat spikar could be further classified into three isoforms: spikar A (isolated in this study, accession number AB074010), spikar B (XP_215942), and spikar delta-C (isolated in this study, AB721962) (Fig. 1a). Spikar contains a NLS, Plant Homeo Domain, Bromo domain, nuclear receptor recognition sequence (a LXXLL motif), PWWP domain, coiled-coil domain, and a MYND domain (Fig. 1a). In the following experiments, we used spikar A unless explicitly stated otherwise.

BS69 is a spikar-like protein containing Plant Homeo Domain, Bromo, PWWP, coiled-coil, and MYND domains (Fig. 1a), and is a co-repressor of transcription (Masselink and Bernards 2000). Because spikar has a domain structure similar to BS69, we used a reporter gene assay to examine whether spikar affects transcription in the kidney fibroblast cell line CV1. When spikar was co-transfected with thyroid hormone receptor β1 (TRβ1), spikar potentiated TRβ1-mediated transcription of thyroid hormone response element in the presence of its ligand, triiodothyronine (T3; Fig. 1b). This activation was induced by T3 and was dependent on the spikar dose, indicating that spikar is a transcriptional co-activator for TRβ1 activity. This co-activator activity of

spikar was also detected in the neuroblastoma cell line N2A (Fig. 1c). In addition, spikar activated transcription mediated by the glucocorticoid receptor and estrogen receptor α (Figure S4a and b), both of which are expressed in the hippocampus (Tohgi *et al.* 1995). These data suggest that spikar acts as a transcriptional co-activator for nuclear receptors in these cells.

Spikar and drebrin interact at their N-terminal regions

We examined whether full-length drebrin binds to full-length spikar using a pull-down assay. His^6-drebrin specifically pulled down GFP-spikar from lysates of cells expressing GFP-spikar (Fig. 1d), demonstrating that drebrin can bind to spikar *in vitro*.

Next, we identified the spikar-binding region of drebrin using a yeast two-hybrid assay with drebrin (1–134) and drebrin (135–233). This assay showed that drebrin (1–134) bound to spikar, but drebrin (135–233) did not (Figure S5a). We then constructed a series of deletion derivatives of spikar to determine which region is required for the interaction with drebrin (1–134). Spikar (88–376), which contains the N-terminal region of spikar, bound strongly to drebrin (1–134). In contrast, spikar (384–1208) did not bind to drebrin. Because spikar (88–258) showed no significant binding activity, and spikar (146–376) showed only weak binding activity (Figure S5b), it appears that spikar (88–376) is necessary for strong drebrin-binding activity. A pull-down assay also demonstrated that full length HA-spikar as well as HA-spikar (1–376) bound to GST-drebrin (1–138), but HA-spikar (377–1208) did not (Fig. 1e). These data were consistent with the results of the yeast two-hybrid assay.

Immunochemical analysis of spikar expression

Immunoblot analysis of protein extracts prepared from various adult rat tissues showed that spikar was ubiquitously detected in the brain, spinal cord, thymus, liver, kidney, spleen, lung, heart, and testis, although the expression levels varied among the tissues (Fig. 1f). Notably, spikar expression levels were high in the thymus and spleen. In the central nervous system, spikar expression was greater in the cerebellum than the cerebral cortex and the spinal cord; spikar was hardly detected in glial cultures (Fig. 1g).

We next examined the subcellular distribution of spikar in cerebral cortex homogenate. Spikar was recovered mainly in the P1 fraction, which includes the cell nuclei. A small amount of spikar was also recovered in the P3 (microsomal) fraction (Fig. 1h). Drebrin was also recovered in the P3 fraction. To characterize the association of spikar with the P3 fraction, we treated the P3 fraction with detergent or a high salt solution. Spikar was detected in the cytosolic fraction formed by treatment with a high concentration of salt (1 M NaCl), whereas only faint amounts were detected in the cytosolic fraction formed by treatment with 1% Triton X-100 (Fig. 1i). As an internal control for membrane protein, we used an immunoglobulin binding protein (Bip), which was solubilized by 1% Triton X-100 but not by 1 M NaCl. These results indicate that spikar was recovered in the P3 fraction owing to protein–protein, but not protein–membrane, interactions.

Localization of spikar in neuronal nuclei and dendritic spines

Although spikar immunostaining was observed in most brain regions, intense immunostaining was particularly observed in regions with high cellular densities, such as the granule cell and pyramidal layers of the hippocampus and the granular layer of the cerebellum (Fig. 2a). Higher magnification images showed that spikar immunostaining was observed in cell nuclei as well as in a punctate staining pattern along dendrites (Fig. 2b and c).

Similarly, immunocytochemical analysis of hippocampal neurons cultured for 21 DIV showed that spikar immunostaining was present in cell nuclei and distributed along dendrites in a punctate pattern (Fig. 2d, left panels). Spikar immunopositive puncta were also stained with antibodies against drebrin (Fig. 2d, right panels). In the dendritic shaft of developing neurons, spikar was localized mainly in dendritic shaft at DIV 7 but in dendritic spines at DIV 14 (Figure S6). Furthermore, GFP-spikar expressed in cultured neurons accumulated in the nuclei and co-localized with drebrin (Fig. 2e). Because these data indicated that spikar is present in the spine and karyoplasm, we named the protein spikar.

Spikar knockdown decreases spine density during development

We next analyzed the role of spikar in dendritic spine formation. To reduce the expression of spikar, we used two short hairpin RNAs (shRNAs; pSUPER-RNAi-2 and -3) that targeted different regions of spikar mRNA. Both effectively suppressed the exogenous expression of myc-spikar in HEK293 cells (Fig. 3a). In cultured hippocampal neurons, the immunofluorescence intensity of endogenous spikar in the nucleus was decreased to 20% of control by 96 h after transfection with pSUPER-RNAi-3 (spikar-shRNA-3; Fig. 3b and c).

We knocked down spikar at 3 DIV and analyzed the effect on morphogenesis of dendritic protrusions at 16 DIV. We selected transfected neurons by GFP expression. Neuronal morphology was visualized by GFP fluorescence (Fig. 3d). Spikar knockdown (KD) caused a significant decrease in the density of dendritic spines and filopodia at 16 DIV (Control: 43.7 ± 1.8 spines/100 μm; 19.4 ± 1.2 filopodia/100 μm; Spikar KD: 20.6 ± 1.1 spines/100 μm; 11.6 ± 0.9 filopodia/100 μm; $*p < 0.01$; Fig. 3e–g). Interestingly, cumulative frequency distributions showed no differences between the lengths and widths of dendritic spines in spikar-KD and control neurons (Fig. 3h, i), indicating that spikar KD does not affect spine morphology.